Downloaded from http://jgs.lyellcollection.org/ by GSL Maintenance User on July 7, 2021

Research article

JGS
Journal of the Geological Society

https://doi.org/10.1144/jgs2020-207 | Vol. 178 | 2021 | jgs2020-207

Accommodation of India–Asia convergence via strike-slip faulting and block rotation in the Qilian Shan fold–thrust belt, northern margin of the Tibetan Plateau

Feng Cheng[1,2*], Andrew V. Zuza[1], Peter J. Haproff[3], Chen Wu[4], Christina Neudorf[5], Hong Chang[6], Xiangzhong Li[7] and Bing Li[8,9]

[1] Nevada Bureau of Mines and Geology, University of Nevada, Reno, NV 89557, USA
[2] Key Laboratory of Deep-Earth Dynamics of Ministry of Natural Resources, Institute of Geology, Chinese Academy of Geological Sciences, Beijing 100037, China
[3] Department of Earth and Ocean Sciences, University of North Carolina, Wilmington, NC 28403, USA
[4] Key Laboratory of Continental Collision and Plateau Uplift, Institute of Tibetan Plateau Research, Center for Excellence in Tibetan Plateau Earth Sciences, Chinese Academy of Sciences, Beijing 100101, China
[5] Division of Earth and Ecosystem Sciences, Desert Research Institute, 2215 Raggio Parkway, Reno, NV 89512, USA
[6] State Key Laboratory of Loess and Quaternary Geology, Institute of Earth Environment, Chinese Academy of Sciences, Xi'an 710061, China
[7] Yunnan Key Laboratory of Earth System Science, Yunnan University, Kunming 650500, China
[8] Chinese Academy of Geological Sciences, Beijing 100037, China
[9] SinoProbe Center, Chinese Academy of Geological Sciences and China Geological Survey, Beijing 100037, China
FC, 0000-0001-8734-6183; AVZ, 0000-0001-6130-5121; PJH, 0000-0002-3119-2290; CN, 0000-0002-4449-2655; HC, 0000-0002-2279-437X; XL, 0000-0003-3491-8824; BL, 0000-0003-3461-4265
* Correspondence: cfcf.chengfeng@gmail.com

Abstract: Existing models of intracontinental deformation have focused on plate-like rigid body motion v. viscous-flow-like distributed deformation. To elucidate how plate convergence is accommodated by intracontinental strike-slip faulting and block rotation within a fold–thrust belt, we examine the Cenozoic structural framework of the central Qilian Shan of northeastern Tibet, where the NW-striking, right-slip Elashan and Riyueshan faults terminate at the WNW-striking, left-slip Haiyuan and Kunlun faults. Field- and satellite-based observations of discrete right-slip fault segments, releasing bends, horsetail termination splays and off-fault normal faulting suggest that the right-slip faults accommodate block rotation and distributed west–east crustal stretching between the Haiyuan and Kunlun faults. Luminescence dating of offset terrace risers along the Riyueshan fault yields a Quaternary slip rate of *c.* 1.1 mm a^{-1}, which is similar to previous estimates. By integrating our results with regional deformation constraints, we propose that the pattern of Cenozoic deformation in northeastern Tibet is compatible with west–east crustal stretching/lateral displacement, non-rigid off-fault deformation and broad clockwise rotation and bookshelf faulting, which together accommodate NE–SW India–Asia convergence. In this model, the faults represent strain localization that approximates continuum deformation during regional clockwise lithospheric flow against the rigid Eurasian continent.

Supplementary material: Luminescence dating procedures and protocols is available at https://doi.org/10.17605/OSF.IO/CR9MN

Thematic collection: This article is part of the Fold-and-thrust belts and associated basins collection available at: https://www.lyellcollection.org/cc/fold-and-thrust-belts

Received 8 November 2020; **revised** 22 January 2021; **accepted** 25 January 2021

Plate tectonics is complicated by intracontinental deformation due to the continental lithosphere's inherent weakness compared with the oceanic lithosphere (Chen and Molnar 1983) and vertical heterogeneity that can lead to lithospheric decoupling and the propagation of detachment horizons (Burchfiel *et al.* 1989; C.S. Wang *et al.* 2011; Mouthereau *et al.* 2013). As a result, continental plate boundaries are often not expressed as single fault systems, but rather wide (hundreds to thousands of kilometres) zones of diffuse deformation that accommodate relative plate motion, such as the Himalaya–Tibet orogen and the San Andreas–Basin and Range system of western North America (Atwater 1970; Davis and Burchfiel 1973; Molnar and Tapponnier 1975; Flesch *et al.* 2000; Yin 2010; Thatcher *et al.* 2016). Whether continental tectonics can be quantified by plate-like rigid body motion (Luyendyk *et al.* 1980; Tapponnier *et al.* 1982; Weldon and Humphreys 1986; Avouac *et al.* 1993; Meade and Hager 2005; Meade 2007) or viscous-flow-like distributed deformation (England and Houseman 1986; Yin and Taylor 2011; Haproff *et al.* 2018) remains a fundamental question.

With regard to the Himalaya–Tibet orogen and the western North American Cordillera, this question focuses on whether major faults such as the left-slip Altyn Tagh fault and the right-slip San Andreas fault act as discrete boundaries of internally rigid crustal blocks or simply localized zones of high strain within a larger deforming continuum (Tapponnier *et al.* 1982; England and Houseman 1986; Avouac *et al.* 1993; Platt and Becker 2010; Johnson 2013; Platt and Becker 2013; Evans *et al.* 2016). A better understanding of the kinematic history of the strike-slip fault systems across the Himalaya–Tibet orogen allows us to explore their role in accommodating India–Asia plate convergence and answer the question of discrete v. distributed intracontinental deformation.

The Qilian Shan fold–thrust belt marks the northeastern margin of the Tibetan Plateau (Fig. 1a) and is bounded by the internally

© 2021 The Author(s). Published by The Geological Society of London. All rights reserved. For permissions: http://www.geolsoc.org.uk/permissions.
Publishing disclaimer: www.geolsoc.org.uk/pub_ethics

Downloaded from http://jgs.lyellcollection.org/ by GSL Maintenance User on July 7, 2021

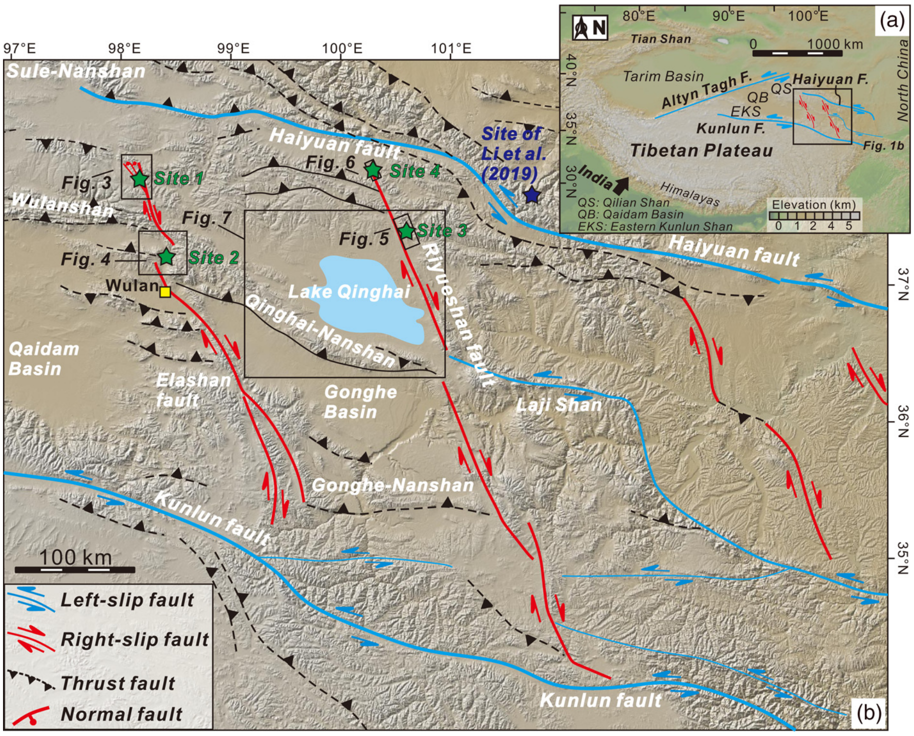

Fig 1. (**a**) Map of the Himalaya–Tibet orogen showing major strike-slip faults in northeastern Tibet. (**b**) Map of the Qilian Shan region showing major strike-slip and thrust faults. Base maps were generated using GeoMapApp (www.geomapapp.org) (Ryan *et al.* 2009). The geometry and kinematics of the faults are derived from Zuza *et al.* (2016) and Taylor and Yin (2009).

rigid Tarim and Qaidam basins to the WSW and the North China craton to the NE (Braitenberg *et al.* 2003; Guo *et al.* 2005; Kusky and Mooney 2015; Cheng *et al.* 2017; Xu *et al.* 2020). The fold–thrust belt has accommodated Cenozoic India–Asia convergence through a combination of NE-directed shortening and NW- and WNW-striking strike-slip faulting (Dewey and Burke 1973; Tapponnier *et al.* 1990; Gaudemer *et al.* 1995; Murphy *et al.* 1997; Métivier *et al.* 1998; Meyer *et al.* 1998; Yin and Harrison 2000; Yin *et al.* 2008*a*; Taylor and Yin 2009; Yin 2010; Zuza *et al.* 2016; Allen *et al.* 2017; Cheng *et al.* 2019*b*). Major WNW-striking left-slip faults in the Qilian Shan (i.e. the Haiyuan fault) and the Kunlun fault to the south are considered to behave as the respective northern and southern boundaries of clockwise-rotating crustal blocks (Fig. 1b) that resemble a bookshelf fault system (England and Molnar 1990; Zuza *et al.* 2016). Crustal blocks are bounded to the east and west by NNW-striking right-slip faults such as the Riyueshan and Elashan faults (Fig. 1b).

Over the last few decades, geological and geophysical studies have improved our understanding of the geometry and kinematics of Cenozoic deformation in the Qilian Shan fold–thrust belt (Zhang *et al.* 2004; Ghosh *et al.* 2006; Bovet *et al.* 2009; Zheng *et al.* 2010; Yin and Taylor 2011; Zuza *et al.* 2016; Pan *et al.* 2020). Despite disagreement regarding the Cenozoic growth history of the Qilian Shan (Bovet *et al.* 2009; Allen *et al.* 2013; He *et al.* 2018; Zuza *et al.* 2018*a*; Cheng *et al.* 2019*b*; Li *et al.* 2020*b*), most studies agree that strike-slip faulting has been active since the Mid-Miocene (Lin *et al.* 2011; W.-T. Wang *et al.* 2011; X. Wang *et al.* 2011; Duvall *et al.* 2013; Li *et al.* 2019). However, the mechanism that generated the sets of NW-striking right-slip faults and WNW-striking left-slip faults and their kinematic evolution since the Mid-Miocene remain inadequately understood (Wang and Burchfiel 1997; Duvall and Clark 2010; Yuan *et al.* 2013).

Continental strike-slip faults are commonly accompanied by a variety of structures, including horsetail splay faults at their tips, local contractional faults at restraining bends, local extensional faults at releasing bends and bookshelf faults (Fig. 2) (Cunningham and Mann 2007; Duvall *et al.* 2013; Zuza and Yin 2016). In addition, the geometric arrangement of Riedel shears and associated structures along strike-slip faults can provide information on the kinematics within the wrench zone (Fig. 2) (Bartlett *et al.* 1981). Here, we integrate the results of satellite imagery analysis and geological field mapping along the right-slip Elashan and Riyueshan faults and existing temporal constraints of deformation associated with these faults to evaluate the mechanism(s) that drove the strike-slip faulting and block rotation in the Qilian Shan. By combining measurements of offset terrace risers along the right-slip Riyushan fault with the luminescence ages of terraces, we determine a late Quaternary slip rate of *c.* 1.1 mm a^{-1}. Using these results, we discuss the late Cenozoic evolution of the Qilian Shan, which informs how intra-thrust belt block rotation and strike-slip faulting accommodate plate convergence.

Geological setting

Pre-Cenozoic tectonic evolution of the Qilian Shan

The pre-Cenozoic tectonic evolution of the Qilian Shan orogen consists of Neoproterozoic continental break-up, Early Paleozoic subduction and subsequent continental collision, followed by Mesozoic extension (Yin and Harrison 2000; Yang *et al.* 2001; Yin *et al.* 2007; Song *et al.* 2009; Xiao *et al.* 2009; Song *et al.* 2013; Huang *et al.* 2015; T. Wang *et al.* 2016; Cheng *et al.* 2017; C. Wang *et al.* 2017; Wu *et al.* 2017; Zuza *et al.* 2018*b*; Cheng *et al.* 2019*c*). Precambrian basement rocks are sporadically exposed in the Qilian Shan and record the tectonic–magmatic events related to the early Neoproterozoic subduction between the South Tarim–Qaidam and North Tarim–North China continents and subsequent late Neoproterozoic continental rifting (Wan *et al.* 2001; K. Tung *et al.* 2007; Song *et al.* 2012; K.-A. Tung *et al.* 2013; Zuza *et al.* 2018*b*; Cheng *et al.* 2019*a*; Cheng *et al.* 2019*b*).

The Qilian Shan orogen also contains early Paleozoic flysch sequences, plutons, ophiolitic mélange and metamorphic rocks. These rocks record the early Paleozoic closure of the Qilian Ocean as the Kunlun–Qaidam terrane collided with the North China craton (Song *et al.* 2009; Xiao *et al.* 2009; Wu *et al.* 2017). Mesozoic strata overlie Paleozoic strata and Precambrian basement (Zuza *et al.* 2018*b*). Triassic plutons that intrude the Paleozoic strata and Precambrian basement probably record the Mesozoic closure of the

Downloaded from http://jgs.lyellcollection.org/ by GSL Maintenance User on July 7, 2021

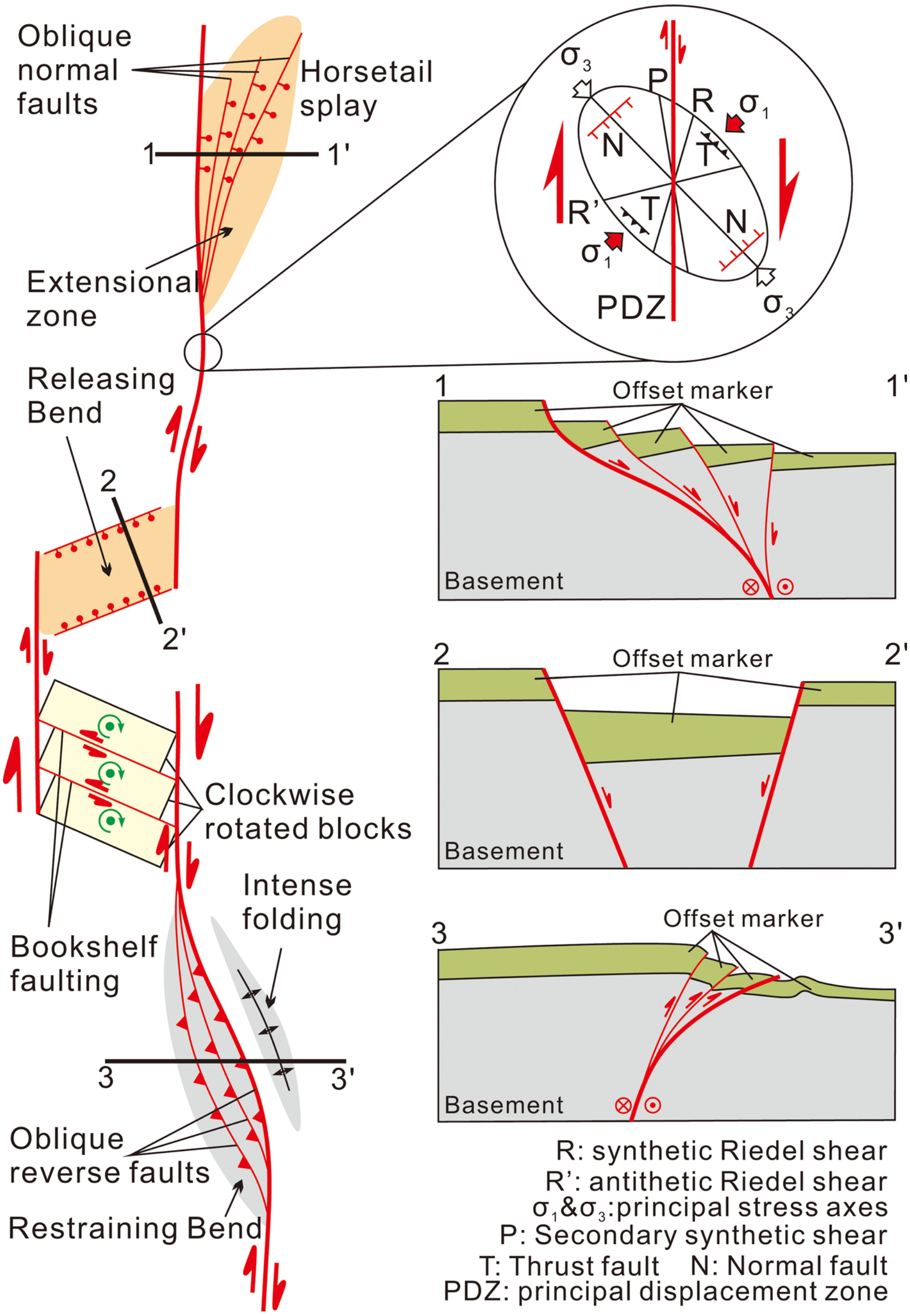

Fig 2. Diagram showing various types and orientations of structures as part of a larger non-linear strike-slip fault system. Note the horsetail splay, restraining bend, releasing bend and bookshelf fault system. Also shown is Riedel's model of faults within a larger strike-slip fault zone, showing the local stress field and geometric relations between structures formed in a simple shear regime. Modified from Davis *et al.* (2000).

Palaeotethys and Mesotethys oceans (Pullen *et al.* 2008; L. Yu *et al.* 2017). Slab rollback in the south and shearing along the Altyn Tagh fault zone (Cheng *et al.* 2019*c*) might have led to regional extension in the Qilian Shan during the Jurassic–Cretaceous.

As summarized by Zuza *et al.* (2018*b*) and Wu *et al.* (2016), the pre-Cenozoic history of this orogen is still ambiguous, with current disputes focused on the polarity of oceanic subduction, the number and location of suture zones, and the onset timing and duration of orogenesis. Several disparate belts of suture zone material are exposed in the Qilian Shan, which form zones of pre-existing weakness that were reactivated in the Cenozoic (Zuza *et al.* 2018*b*; Li *et al.* 2020*a*).

Cenozoic tectonic evolution of the Qilian Shan

Cenozoic structures of the Qilian Shan consist of series of NW-striking fold–thrust belts and the WNW-striking, left-slip Haiyuan and Kunlun faults (*c.* 100–110° strike) (Fig. 1b). Several NNW-striking right-slip faults, including the Elashan and Riyueshan faults, are located at high angles between the Haiyuan fault to the north and the Kunlun fault to the south (Fig. 1b) (Meyer *et al.* 1998; Yin *et al.* 2008*b*; Lease *et al.* 2011; Lease 2014; Cheng *et al.* 2015*b*; Zuza *et al.* 2016; Allen *et al.* 2017).

As indicated by existing low-temperature thermochronological data and sedimentological records, the southern part of Qilian Shan experienced significant crustal shortening during the Paleocene to Eocene shortly after India–Asia collision, followed by Oligocene exhumation of the central and northern parts of the Qilian Shan (Jolivet *et al.* 2001; Bovet *et al.* 2009; Zhuang *et al.* 2011; He *et al.* 2017; He *et al.* 2018; Cheng *et al.* 2019*b*). Given the general northwards younging initiation ages of Cenozoic structures within the Qilian Shan, some studies advocate for a progressive northwards propagation of deformation from the Miocene to Pliocene (George *et al.* 2001; Bovet *et al.* 2009; D. Zheng *et al.* 2010, 2017; W. Wang *et al.* 2016; Cheng *et al.* 2019*b*). However, several pulses of out-of-sequence thrusting have been reported throughout the Qilian Shan (Zuza *et al.* 2018*a*; Li *et al.* 2020*b*). Aside from the NE–SW-directed shortening across the Qilian Shan fold–thrust belt, the

Downloaded from http://jgs.lyellcollection.org/ by GSL Maintenance User on July 7, 2021

>1000 km long, WNW-striking, left-slip Haiyuan fault (Fig. 1) probably played an important part in accommodating crustal deformation in northeastern Tibet from the Mid-Miocene (Burchfiel *et al.* 1991; Duvall *et al.* 2013; Yuan *et al.* 2013; Zuza *et al.* 2016; Li *et al.* 2019).

Rotating bookshelf faulting

The Elashan and Riyueshan faults are sub-parallel, NW-striking (*c.* 325–340° strike), right-slip faults situated between the left-slip Haiyuan fault to the north and the left-slip Kunlun fault to the south, forming a rotating bookshelf fault system (Fig. 1b). Slip initiated along the Elashan and Riyueshan faults at 9 ± 3 and 10 ± 3 Ma, respectively (Duvall *et al.* 2013; Yuan *et al.* 2013). The reported late Quaternary slip rates along the middle segments of the Elashan and Riyueshan faults are 1.1 ± 0.3 and 1.2 ± 0.4 mm a^{-1}, respectively (Yuan *et al.* 2011).

Methods

Geological field mapping, satellite image analysis and seismic profile interpretation

To investigate the geometry and kinematics of the structures within the Qilian Shan, we conducted geological field mapping along the Riyueshan and Elashan faults within the central part of the Qilian Shan fold–thrust belt (sites 1, 2, 3 and 4 in Fig. 1b). Detailed field observations across much of the Qilian Shan have been reported previously (Wu *et al.* 2017; Zuza *et al.* 2018*a*; Zuza *et al.* 2018*b*; Cheng *et al.* 2019*a*). Google Earth imagery and field observations were used to document the surface trace and kinematics of these two faults. In addition, we reinterpreted a previously published seismic reflection profile across Lake Qinghai adjacent to the Riyueshan fault (Fig. 1b) (An *et al.* 2006) to further understand the kinematics of the bookshelf faults.

Luminescence geochronology

Two samples (RF001 and RF002) were collected for optically simulated luminescence dating from one site (site 4) along the northern segment of the Riyueshan fault near its termination at the Haiyuan fault (Fig. 1b). Sample RF001 was collected from a north-facing wall along the south side of a stream drainage at a depth of 85 cm below the channel-incised wall or riser (site 4a). Sample RF002 was collected south of sample RF001 from the north-facing wall along the south side of a stream drainage at a depth of 65 cm below the channel-incised wall (site 4c). The sampled sediment is mainly composed of massive pebbly silty clay with rootlets extending 90 cm below the ground surface and the uppermost 20–25 cm consists of modern day soil. Angular pebbles appear to be locally derived and therefore the sediments are probably colluvial with an aeolian component.

Samples RF001 and RF002 were collected by hammering steel tubes into the cleaned surfaces of the terrace walls. The tubes were subsequently removed from the terrace wall and wrapped in light-proof plastic for transport to the Desert Research Institute E.L. Cord Luminescence Laboratory (Reno, NV, USA) for further sample preparation. Detailed sample preparation and analytical procedures are described in the Supplementary Material.

Initial luminescence measurements and dose recovery tests showed that potassium-rich feldspar (Brookfield) grains were better suited to dating than the quartz grains in these samples (see Supplementary Material for details). Infrared-stimulated luminescence (IRSL) ages were therefore measured from small (1 mm diameter) aliquots of fine sand-sized grains. The age distributions from *c.* 45 measurements from both samples were tight with an overdispersion of <10%. This indicates that the measured fine sand-sized feldspar grains were well bleached prior to burial. We therefore interpret an aeolian origin for much of the sediment and/or shallow slope aggradation, which supports an aeolian and/or shallow colluvial origin for the deposit.

Results of field- and satellite-based observations

Elashan fault

The northern tip of the Elashan fault is expressed as a horsetail splay structure consisting of a series of NW- to NNW-striking faults that merge to the south (site 1, Fig. 3a). Regional geological maps show that these faults offset Triassic shallow marine and terrestrial strata along a right-slip sense (Fig. 3b, c) (Qinghai-Geology-Bureau 1976). By contrast, the northwesternmost tip of the Elashan fault features minor faults with both right-slip and left-slip separation (Fig. 3d, e). Previous geological mapping (Qinghai-Geology-Bureau 1976) and satellite-based observations suggest that these structures are high-angle faults as a result of their relatively linear traces across the topography and the displacement of gently SW-dipping strata (Fig. 3d, e). We suggest that the right-slip and left-slip map view separation along these faults reflects dominantly dip-slip normal kinematics.

To the south of site 1, just north of the city of Wulan (site 2, Fig. 1b), the middle segment of the Elashan fault has two right-stepping releasing bends that form a local pull-apart basin featuring several north- and NNW-striking faults (Fig. 4a, b). The north-striking fault traces are sub-parallel to the trend of the local river drainage and several triangular facets are observed along the faults (Fig. 4a, b). In addition, the north-striking linear faults do not laterally displace the local stream drainage (Fig. 4a) or topography (Fig. 4b). We therefore interpret the north-striking faults to have dominantly dip-slip kinematics. By contrast, the NW-striking faults feature sub-horizontal striations in vertical fault planes (Fig. 4d), suggesting dominantly strike-slip kinematics (Fig. 4e).

Riyueshan fault

The northern segment of the Riyueshan fault shows a complex variability between strike-slip and normal-slip kinematics. The Riyueshan fault along the western flank of the Lakeshan Range (site 3 on Fig. 1b), which strikes *c.* 338°, features triangular facets and displays no evidence of laterally displaced stream drainage (Fig. 5), which suggests dominantly dip-slip kinematics. However, the northernmost segment of the Riyueshan fault (site 4 on Fig. 1b), which strikes *c.* 328°, features right-laterally displaced stream drainage (Fig. 6a). We did not observe any dip-slip displacement at this latter site. This structural geometry is similar to that of the Elashan fault, wherein the more northerly striking fault segments have normal-slip normal kinematics segments, whereas the fault segments with a more NW-striking orientation have strike-slip kinematics.

At the northernmost site along the Riyueshan fault, we surveyed right-laterally displaced fluvial terrace risers at three locations (sites 4a–4c, Fig. 6a). To mitigate potential errors in measuring the displaced fluvial terrace risers (Cowgill 2007), we systematically measured the right-lateral displacements of the thalweg and bounding risers on both sides of the drainage to determine a range of plausible displacement magnitudes. Based on riser morphology, we report an average displacement magnitude and standard deviation (1σ), which typically excludes measurements of rounded, eroded and/or ambiguous riser crests.

At site 4a, we determined that the northern riser, thalweg and southern riser are displaced by 7.41, 8.04 and 5.60 m, respectively (Fig. 6b). At site 4b, we determined that the northern riser, thalweg and southern riser are displaced by 9.45, 7.66 and 5.63 m, respectively (Fig. 6c). At site 4c, the northern riser, thalweg and

Downloaded from http://jgs.lyellcollection.org/ by GSL Maintenance User on July 7, 2021

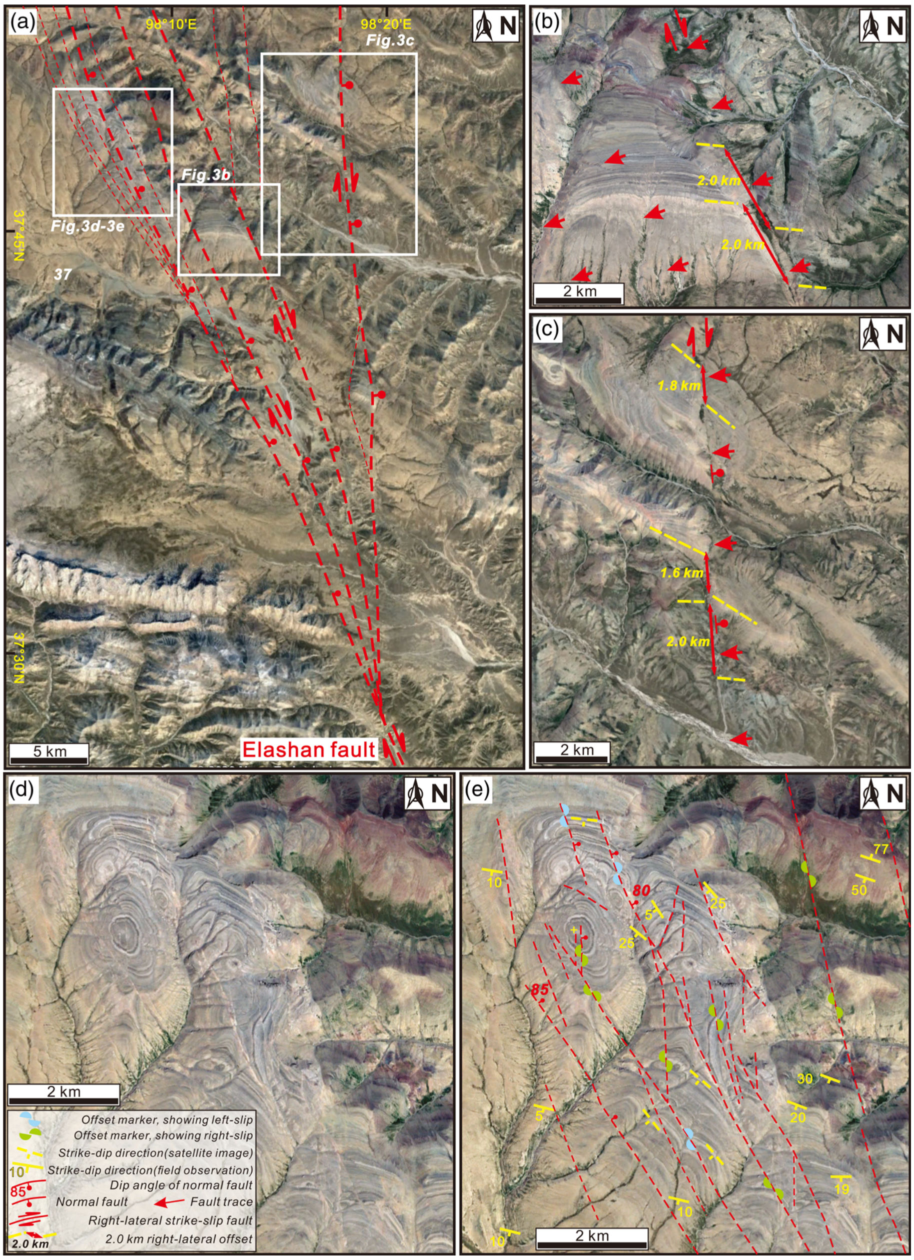

Fig 3. Google Earth based map (© 2021 Maxar Technologies) of faults along the northern segment of the Elashan fault. (**a**) Horsetail splay structure, (**b**, **c**) right-slip displacement of Triassic strata and (**d**, **e**) several subsidiary faults cutting Triassic strata. The locations of the maps are shown in Figure 1b.

southern riser are displaced by 8.30, 7.90 and 8.85 m, respectively (Fig. 6d). The average (1σ) right-slip displacement magnitudes along the Riyueshan fault at sites 4a, 4b and 4c are 7.73 ± 0.45 m (Fig. 6b), 8.56 ± 1.27 m (Fig. 6c) and 8.10 ± 0.28 m (Fig. 6d), respectively. Erosion and degradation of the southern risers at each site added to the uncertainty of the displacement measurements. For this reason, our reported average displacement estimates exclude the displacement measurements of the southern risers.

Results of geophysical observations

A previous geophysical survey by An *et al.* (2006) across Lake Qinghai (Fig. 1b) shows a series of WNW-striking, high-angle faults (Fig. 7). By comparing the isobaths of subsurface reflectors on either side of these faults, we observed that the faults have both apparent right-slip and left-slip separation (Fig. 7) and divide the Lake Qinghai Basin into several internally rigid blocks (Fig. 7a).

The orientation of these WNW-striking, high-angle faults compared with the larger WNW-striking Haiyuan fault to the north and the Kunlun fault to the south are roughly consistent with the expected orientation of subsidiary normal faults parallel to the minimum compressive stress within a strike-slip system (Fig. 7b). In a north–south-trending seismic reflection profile, we observe sets of growth strata that indicate a >5 Ma initiation timing of normal faulting (Fig. 7c) (Fu *et al.* 2013).

Results of luminescence geochronology and slip rate of the Riyueshan fault

Samples RF001 and RF002 yield respective IRSL ages of 7.15 ± 0.42 and 7.16 ± 0.42 ka (Table 1). The nearly identical IRSL ages of samples RF001 and RF002, despite being collected *c.* 550 m apart from two displaced stream drainages (Fig. 6), suggest spatially uniform erosion and aggradation processes over time and relatively minor aggradation during most of the Holocene. Both samples were taken within a metre of the ground surface and below the soil horizon and no paleosol was observed at depth in the terrace walls. It is therefore possible that aggradation rates were higher in the late Pleistocene–early Holocene before slowing at *c.* 7 ka. Assuming that the sampled sediments aggraded prior to channel incision and fault slip, the average IRSL ages reflect the maximum ages for the most recent displacement along the Riyueshan fault.

Downloaded from http://jgs.lyellcollection.org/ by GSL Maintenance User on July 7, 2021

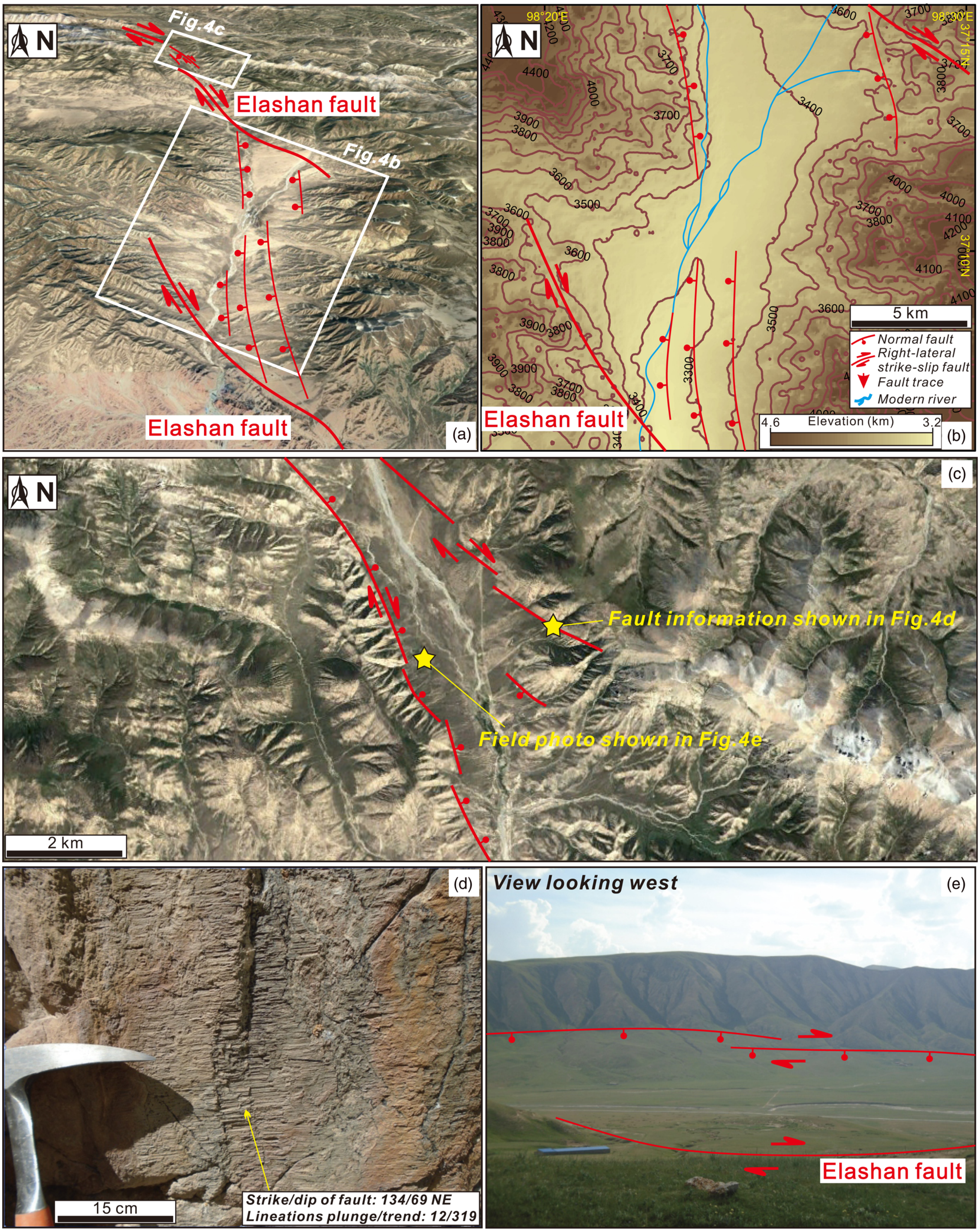

Fig 4. Images of faults and fabrics along the northern segment of the Elashan fault. (**a**) Oblique view Google Earth based image (© 2021 Maxar Technologies) of the pull-apart basin. (**b**) Topographic base map of the pull-apart basin (location shown in Fig. 4a). Note that the river drainage and contour lines are not laterally displaced by the faults, indicating dominant dip-slip kinematics. (**c**) Google Earth based map (© 2021 Maxar Technologies) of a restraining bend along the Elashan fault (location shown in Fig. 4a). (**d**) Field photographs showing the sub-horizontal striations on the Elashan fault surface. (**e**) Field photograph showing strike-slip and normal faults along the Elashan fault.

Given the 7.73 ± 0.45 m displacement and 7.15 ± 0.42 ka IRSL age at site 4a, we determine a late Quaternary slip rate of 1.1 ± 0.1 mm a^{-1} (1σ) along the Riyueshan fault. Given the 8.35 ± 0.47 m displacement and 7.16 ± 0.42 ka IRSL age at site 4c, we determine a late Quaternary slip rate of 1.2 ± 0.1 mm a^{-1} along the Riyueshan fault. We thus estimate the mean late Quaternary slip rate

Downloaded from http://jgs.lyellcollection.org/ by GSL Maintenance User on July 7, 2021

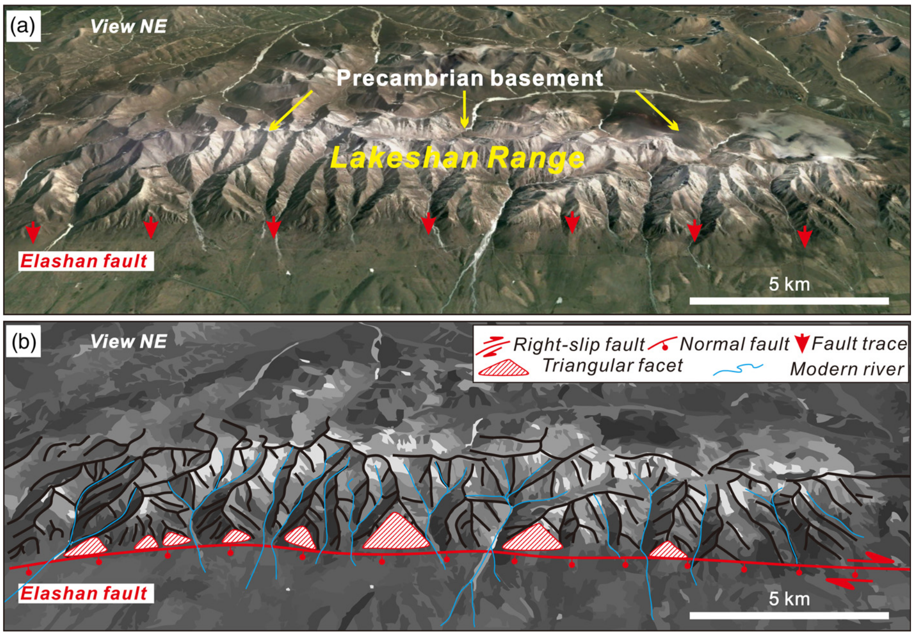

Fig 5. Oblique view Google Earth based images (© 2021 Maxar Technologies) of the northern segment of the Riyueshan fault. (**a**) Linear trace of the Riyueshan fault. (**b**) Annotated sketch map showing the surface trace, triangular facets and undeformed stream channel along the Riyueshan fault.

along the northern part of the Riyueshan fault to be 1.1 ± 0.1 mm a^{-1} (1σ).

Discussion

Strike-slip faulting and block rotation related to the Riyueshan and Elashan faults

Our field- and satellite-based observations allow us to better characterize the geometry and kinematics of the right-slip Elashan and Riyueshan faults. The northwestern termination of the Elashan fault constitutes a horsetail splay fault system (Fig. 3) that probably distributes lateral shear. Directly north of this structure is the western segment of the WNW-striking Haiyuan fault, which is not displaced right-laterally by the Elashan fault (Fig. 1b). This requires right-slip faulting to terminate at the mapped tip of the Elashan fault and not continue northwards across the Haiyuan fault (Fig. 1b). The middle segment of the Elashan fault is expressed as a pull-apart basin (Fig. 4). The northern and middle segments of the Riyueshan fault are right-lateral normal oblique-slip faults. The development of these subsidiary structures suggests that both the Riyueshan and Elashan faults probably accommodated regional extension since their inception. Based on their geometries and transtensional setting, these faults accommodate west–east stretching of Qilian Shan.

Previous studies have inferred that right-lateral slip along the Elashan and Riyueshan faults initiated at 9 ± 3 and 10 ± 3 Ma, respectively (Yuan *et al.* 2011; Duvall *et al.* 2013). The west- to WNW-striking Qinghai–Nanshan and Gonghe–Nanshan thrusts (Fig. 1b), which form kinematically linked thrust ramps between the Elashan and Riyueshan faults, initiated at 11–9 Ma (Zhang *et al.* 2012) and 10–7 Ma, respectively (Craddock *et al.* 2011). This coeval Late Miocene initiation of the timing of deformation (Fig. 8a) implies a regional rather than local driving force, possibly induced by a NE-trending maximum principal compressive stress related to NE–SW India–Asia convergence. As a consequence, right-lateral slip along the Elashan and Riyueshan faults resulted in coeval Miocene extension by the Lake Qinghai fault system in the north and shortening by the Qinghai–Nanshan and Gonghe–Nanshan thrusts (Fig. 1b). A Miocene onset of faulting in the Lake Qinghai fault system is roughly supported by the >5 Ma age revealed by the growth strata (Fig. 7) (Fu *et al.* 2013).

Given that the Miocene onset of left-slip motion along the Kunlun and Haiyuan faults (Jolivet *et al.* 2003; Lin *et al.* 2011; W.-T. Wang *et al.* 2011; X. Wang *et al.* 2011; Duvall *et al.* 2013; Cheng *et al.* 2014; Li *et al.* 2019) is roughly consistent with the initiation ages of the right-slip structures between these left-slip

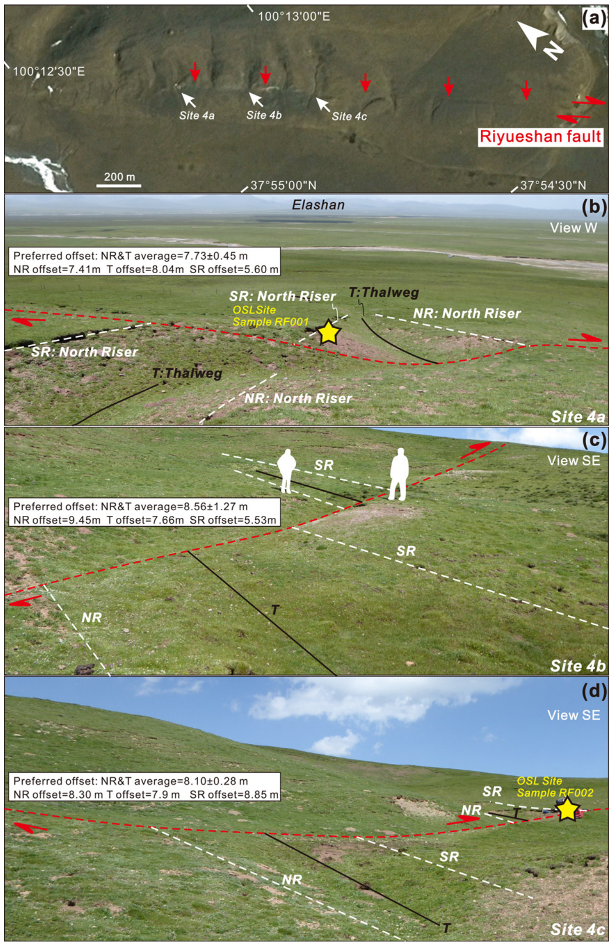

Fig 6. Google Earth based image (© 2021 Maxar Technologies) and field photographs along the northern segment of the Riyueshan fault.
(**a**) Google Earth based image of the fault trace. (**b**–**d**) Field photographs of sites 4a, 4b and 4c with displacement measurements and sample locations. Samples RF001 and RF002 were collected at sites 4a and 4c, respectively, for IRSL dating. Dating results are shown in Table 1.

Downloaded from http://jgs.lyellcollection.org/ by GSL Maintenance User on July 7, 2021

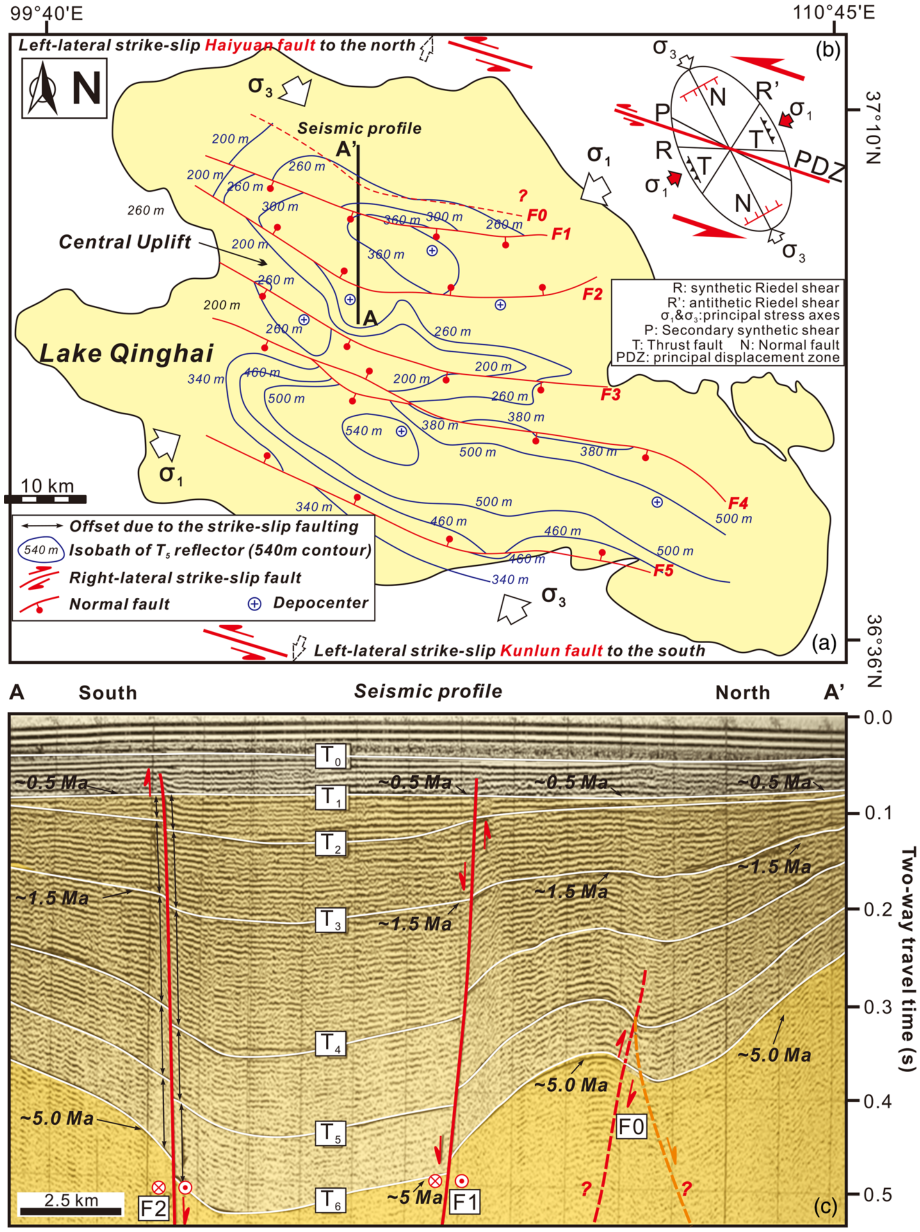

Fig 7. (**a**) Simplified tectonic map, (**b**) Riedel's model of faults, showing the local stress field, and (**c**) seismic profile of the Lake Qinghai fault system, modified from An *et al.* (2006). The ages of the strata are based on magnetostratigraphy data from a Lake Qinghai drilling core (Fu *et al.* 2013) and regional seismic profile correlation. Note that an alternative interpretation that shows a north-dipping normal fault (F_0) is shown in orange. Reprinted from An *et al.* 2006 with permission from Springer Nature.

faults, we propose that the Elashan and Riyueshan right-slip faults initiated in the Miocene as part of a bookshelf fault system embedded within the left-lateral shear zone between the Haiyuan and Kunlun faults (e.g. Duvall and Clark 2010). For a bookshelf fault system that is controlled by a broad left-slip shear zone, the internal fault-bounded blocks are predicted to rotate counterclockwise (Fig. 8b). This kinematic prediction is complicated because northern Tibet is part of a broad NE-trending right-lateral shear zone that experiences clockwise rotation against the fixed Tarim block and left-slip Altyn Tagh fault (Cobbold and Davy 1988; England and Molnar 1990; Zuza and Yin 2016), including the Haiyuan and Kunlun left-slip faults, their fault-bounded wallrock and the right-slip fault system.

Previous palaeomagnetic studies adjacent to this right-slip fault domain between the Haiyuan and Kunlun faults do not yield significant rotation since the Miocene (Dupont-Nivet *et al.* 2003; Fang *et al.* 2003) (Fig. 8a). However, if most of northern Tibet experienced clockwise rotation, local counterclockwise rotation within the bookshelf fault system might be obscured as the integrated rotation magnitudes cancel each other out within uncertainties (Fig. 8c). We therefore propose a hybrid model with regional right-lateral shear and clockwise rotation in northern Tibet that drives left-slip motion along the Haiyuan and Kunlun faults, which ultimately causes smaller scale counterclockwise rotation and right-slip bookshelf faulting between the left-slip faults (Fig. 8d).

Crustal stretching and lateral displacement along strike-slip faults in northern Tibet

It remains debatable whether there has been significant crustal stretching and lateral displacement along strike-slip faults in northern Tibet since the Miocene (Gaudemer *et al.* 1995; Ding *et al.* 2004; Harkins *et al.* 2010; Cheng *et al.* 2015*b*). This type of potential deformation is likely to be limited to the upper crust (Hubbard and Shaw 2009; Tian *et al.* 2016; Shen *et al.* 2019). As shown by recent earthquake focal mechanisms in the Qilian Shan region (Pan *et al.* 2020), most earthquakes are associated with NW-striking reverse faults and strike-slip faults (Fig. 9a). Earthquake focal mechanisms indicate right-slip motion along the Elashan and Riyueshan faults and reverse fault motion along the Qinghai–Nanshan and Gonghe–Nanshan thrusts (Fig. 9a). The recent earthquake activity and geometrical relationships between these faults suggest a kinematic linkage between the reverse faults and the Riyueshan and Elashan faults.

Downloaded from http://jgs.lyellcollection.org/ by GSL Maintenance User on July 7, 2021

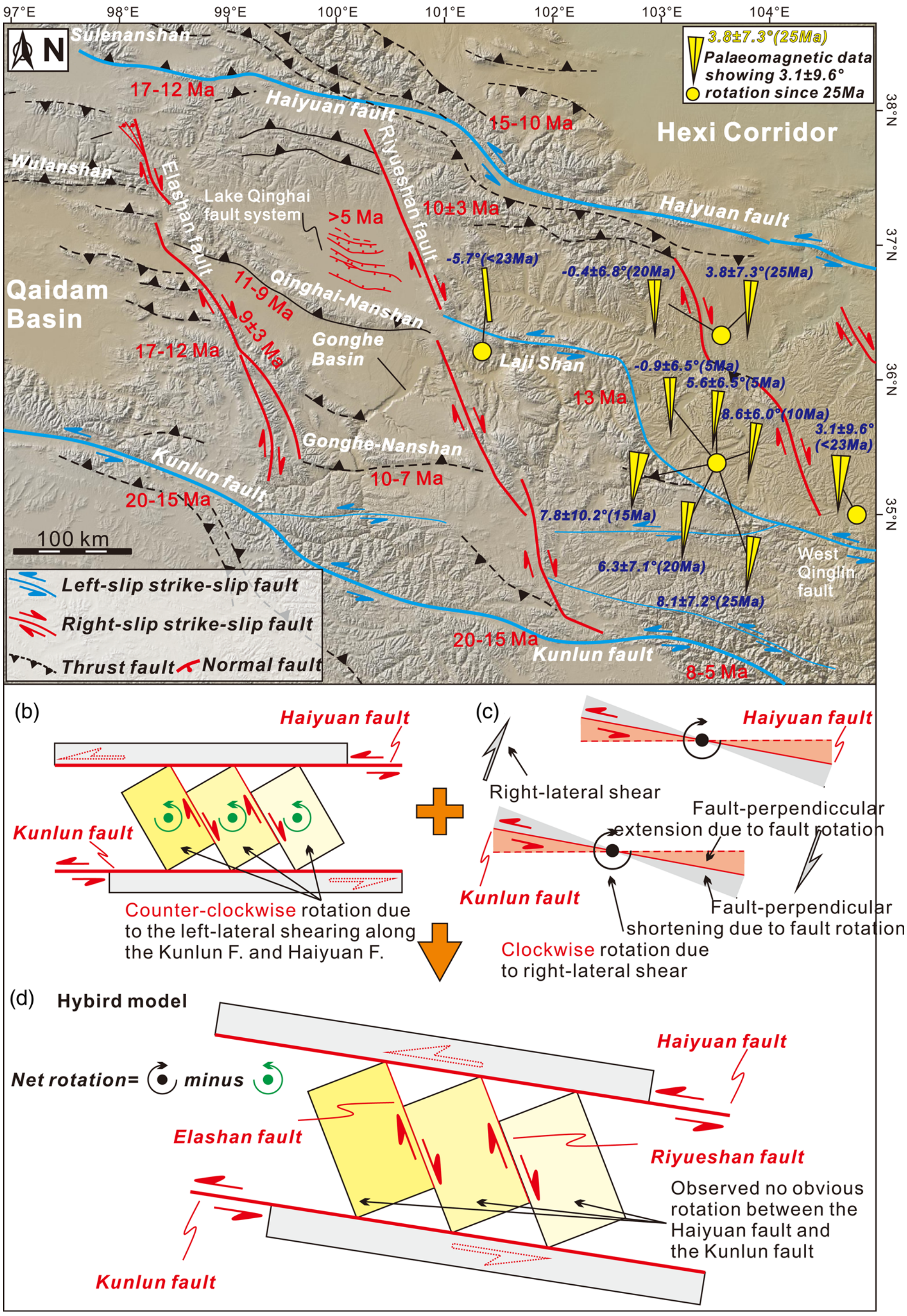

Fig 8. (**a**) Map showing the onset timing of the faulting along the strike-slip faults in northern Tibet. Base map was generated using GeoMapApp (www.geomapapp.org) (Ryan *et al.* 2009). (**b**) Map view diagram showing bookshelf faulting driven by the left-slip motion along the Haiyuan fault to the north and the Kunlun fault to the south. (**c**) Map view diagram showing the regional right-slip shear accommodating the clockwise rotation of northern Tibet (including the Haiyuan and Kunlun faults). (**d**) Hybrid model combining the bookshelf fault model shown in part (b) and the regional right-slip shear model shown in part (c). The onset timing of deformation is compiled from Duvall *et al.* (2013), (Li *et al.* 2019) and references cited therein.

Our field observations and IRSL ages allow us to constrain a late Quaternary average slip rate of 1.1 ± 0.1 mm a^{-1} along the northernmost segment of the Riyueshan fault. This estimate is consistent with the previously estimated late Quaternary slip rates of 1.2 ± 0.4 mm a^{-1} along the middle segment of the Riyueshan fault (Yuan *et al.* 2011) and 1.1 ± 0.3 mm a^{-1} along the middle segment of the Elashan fault. We therefore infer that both the Riyueshan and Elashan faults have shared a *c.* 1 mm a^{-1} uniform slip rate since the Late Quaternary. Assuming this constant long-term slip rate, eastwards crustal displacement in the Qilian Shan

Table 1. *IRSL age data for samples RF001 and RF002*

Sample No.	Depth (cm)	Altitude (m)	n*	Overdispersion (%)	D_b (Gy)‡	U (ppm)	Th (ppm)	K	External β dose rate wet (Gy ka^{-1})	External γ rate wet (Gy ka^{-1})	Cosmic dose rate (Gy ka^{-1})‡	Total dose rate (Gy ka^{-1})§	Age (ka)‖
RF001	85	3643	45 (48)	7	27.79 ± 0.38	2.72	14.0	2.74	2.334	1.468	0.345	5.10 ± 0.26	7.15 ± 0.42
RF002	65	3618	46 (48)	6	30.50 ± 0.37	3.03	16.2	3.03	2.611	1.663	0.363	5.59 ± 0.28	7.16 ± 0.42

*n, number of D_e determinations accepted after screening. The total number of aliquots measured is given in parentheses.
†The burial dose, D_b, was determined using the central age model (Galbraith *et al.* 1999) prior to fading correction and the error is the standard error.
‡Cosmic dose rates (Gy ka^{-1}) were calculated according to Prescott and Hutton (1994).
§Dose rates (Gy ka^{-1}) were calculated using the conversion factors of Liritzis *et al.* (2013) and are shown rounded to two decimal places; ages were calculated using values prior to rounding; central values are given for dose rates and errors are incorporated into that given for the total dose rate.
‖Luminescence ages are expressed as thousands of years before AD 2019 and rounded to the nearest 10 years. Error is 1σ. Final ages are corrected for fading using the model of Huntley and Lamothe (2001) and a measured fading rate of 3.03 ± 0.22% decade^{-1}.

Downloaded from http://jgs.lyellcollection.org/ by GSL Maintenance User on July 7, 2021

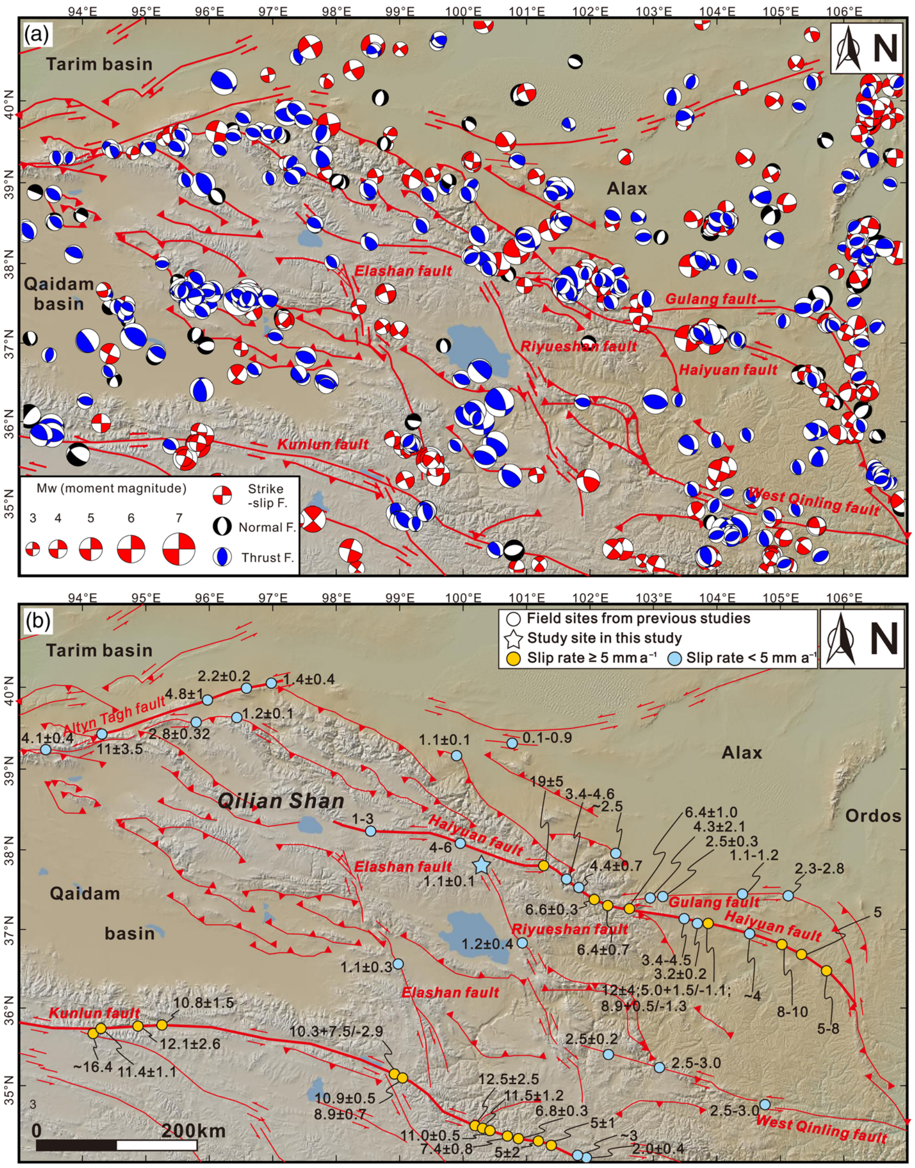

Fig 9. (**a**) Shaded relief map showing recent earthquake focal mechanisms and (**b**) Late Quaternary slip rates along the strike-slip faults of northern Tibet. The earthquake focal mechanism data are from Pan *et al.* (2020) and the slip rate data are compiled from previous studies (Gaudemer *et al.* 1995; Van Der Woerd *et al.* 1998, 2000, 2002; Lasserre *et al.* 1999, 2002; Hetzel *et al.* 2002; H. Li *et al.* 2005; Xu *et al.* 2005; Lin *et al.* 2006; Kirby *et al.* 2007; Liu-Zeng *et al.* 2007; Zhang *et al.* 2007; Harkins and Kirby 2008; Lin and Guo 2008; C. Li *et al.* 2009, 2011; Champagnac *et al.* 2010; Harkins *et al.* 2010; Yuan *et al.* 2011; Zheng *et al.* 2013*a*, 2013*b*, 2013*c*; Luo *et al.* 2015; Gold *et al.* 2017; Jiang *et al.* 2017; J.-X. Yu *et al.* 2017; Elliott *et al.* 2018; Yuan *et al.* 2018; Chen and Lin 2019; Matrau *et al.* 2019; Ren *et al.* 2019; Yao *et al.* 2019; Zhang *et al.* 2019; Pan *et al.* 2020; Shao *et al.* 2020). Base maps were generated using GeoMapApp (www.geomapapp.org) (Ryan *et al.* 2009).

would correspond to >10 km of displacement along each of the right-slip faults.

As shown in the compilation of the Quaternary slip rates in the Qilian Shan region in Figure 9b, the estimated slip rate of the Haiyuan fault ranges from 1–3 to 19 ± 5 mm a^{-1}. However, the study sites of Lasserre *et al.* (1999, 2002), from which faster slip rates of 19 ± 5 and 12 ± 4 mm a^{-1} were derived, have come into question due to a bias towardsthe systematic use of lower terrace reconstructions in interpreting the age of offset (Zheng *et al.* 2013*b*; Yao *et al.* 2019). With the exception of these two possibly overestimated slip rates, the Haiyuan fault slip rates vary from 1–3 to 6.4 ± 0.7 mm a^{-1} along the western fault segment and 3.2 ± 0.2 to 8–10 mm a^{-1} along the eastern fault segment (Li *et al.* 2009; Yuan *et al.* 2011; Zheng *et al.* 2013*b*; Matrau *et al.* 2019; Yao *et al.* 2019). Assuming a constant long-term slip rate (*c.* 4 and *c.* 6 mm a^{-1} along the western and eastern segments, respectively), a left-slip initiation at 15 Ma along the Haiyuan fault (Duvall *et al.* 2013; Li *et al.* 2019; Yu *et al.* 2019) yields *c.* 60–90 km of total displacement. This slip estimate overlaps published offset measurements (Gaudemer *et al.* 1995; Ding *et al.* 2004). For the West Qinling fault, given the estimated slip rate of 2.5–3 mm a^{-1} (Fig. 9b) (Chen and Lin 2019), *c.* 38–45 km of displacement would have occurred since 15 Ma.

Published slip rate estimates for the Kunlun fault are *c.* 16 mm a^{-1} along its western segment and gradually decrease to 8.9 ± 0.7 to 10.9 ± 0.5 mm a^{-1} along its central segment and to 2.0 ± 0.4 mm a^{-1} along its eastern segment (Fig. 9b) (Van Der Woerd *et al.* 1998, 2002; Li *et al.* 2005; Kirby *et al.* 2007; Harkins and Kirby 2008; Lin and Guo 2008; Harkins *et al.* 2010). Assuming a constant long-term slip rate (*c.* 16, 8.9 ± 0.7 to 10.9 ± 0.5 and 2.0 ± 0.4 mm a^{-1} along the western, central and eastern segments, respectively) and left-slip initiations of 12–8, 20–15 and 8–5 Ma along the western, central and eastern segments of the Kunlun fault, respectively, displacement magnitudes of 130–200, 120–230 and 8–20 km would have occurred for these fault segments.

Although the use of a constant slip rate may overestimate or underestimate the total displacement along these faults, these estimates provide a perspective on tens to hundreds of kilometres of eastwards displacement of crust in northern Tibet since the Miocene. Whether these amounts of eastwards displacement of crust in the Qilian Shan along strike-slip faults can be balanced with the magnitude of crustal lateral displacement transferred from >300 km of left-slip displacement along the Altyn Tagh fault (Meyer *et al.* 1998; Searle *et al.* 2011; Cheng *et al.* 2015*b*, 2016*b*) remains uncertain.

The geometries of the Riyueshan and Elashan faults imply that *c.* 1 mm a^{-1} of slip along each fault corresponds to *c.* 0.5 mm a^{-1} of west–east-oriented stretching per fault, or *c.* 1 mm a^{-1} of west–east stretching across the Lake Qinghai fault system. This interpretation based on Quaternary slip rates is comparable with the

Downloaded from http://jgs.lyellcollection.org/ by GSL Maintenance User on July 7, 2021

west–east-oriented stretching rates of 1–2 mm a^{-1} in the same region derived from global positioning system (GPS) velocities (Duvall and Clark 2010). The NE–SW-oriented convergence rate across the central Qilian Shan is 6–7 mm a^{-1} based on a tabulation of shortening estimates over the past 10 Ma (Zuza *et al.* (2018*a*) and *c.* 5–7 mm a^{-1} based on modern convergence rates from GPS velocities (Zhang *et al.* 2004; Gan *et al.* 2007). We therefore infer that, since the Mid- to Late Miocene, the Qilian Shan has accommodated *c.* 6 mm a^{-1} of NE–SW-oriented crustal shortening and slower west–east-oriented stretching of 1–2 mm a^{-1}.

Mechanism of Late Cenozoic deformation in the Qilian Shan

Most studies have reached a consensus that strike-slip faulting in the Qilian Shan fold–thrust belt has been active since the Mid-Miocene (Lin *et al.* 2011; W.-T. Wang *et al.* 2011; X. Wang *et al.* 2011; Duvall *et al.* 2013; Li *et al.* 2019) and accommodated a considerable amount of Cenozoic crustal deformation in northern Tibet (Dewey and Burke 1973; Murphy *et al.* 1997; Yin and Harrison 2000; Dupont-Nivet *et al.* 2002; Yin *et al.* 2002, 2008*a*; E. Wang *et al.* 2006; Taylor and Yin 2009; Yin 2010; Cheng *et al.* 2016*a*; Zuza *et al.* 2016; L. Wang *et al.* 2020).

Two broad end-member models have been proposed to explain this Cenozoic deformation associated with this strike-slip faulting: the eastwards lateral displacement model (Meyer *et al.* 1998; Cheng *et al.* 2015*b*) and the non-rigid passive bookshelf faulting model (Zuza and Yin 2016). The eastwards lateral displacement model emphasizes that the strike-slip faults (e.g. the Kunlun, Haiyuan, Riyueshan, Elashan and West Qinling faults) are the dominant structures in accommodating convergence in northern Tibet. By contrast, the non-rigid passive bookshelf faulting model involves discrete left-slip faulting in northern Tibet, which accommodates distributed off-fault deformation during the regional clockwise rotation of crustal blocks and faults. Despite the merits of the non-rigid passive bookshelf faulting model, it is challenged by palaeomagnetic studies that indicate limited rotation in northern Tibet (Dupont-Nivet *et al.* 2002, 2003; Fang *et al.* 2003; Yu *et al.* 2014) v. others that demonstrate appreciable Neogene clockwise rotation (Cogné *et al.* 1999; Chen *et al.* 2002; Halim *et al.* 2003; Liu *et al.* 2003; Yin *et al.* 2008*a*). The eastwards displacement model is questioned by whether the NW-striking strike-slip faults (e.g. the Riyueshan and Elashan faults) within the Qilian Shan can absorb such a large amount of eastwards crustal motion across northern Tibet (Meyer *et al.* 1998; Cheng *et al.* 2015*b*).

As a result of this study, we suggest that the non-rigid passive bookshelf faulting model can be reconciled with a new integrative model that better explains the kinematics framework of northern Tibet by taking the significant fault-parallel west–east stretching into consideration. We thus propose a hybrid model that combines these two end-member models to describe the Cenozoic deformation pattern of northern Tibet.

In the early Cenozoic, as a result of India–Asia convergence, shortening strain in northern Tibet caused the translation of the Qaidam Basin northwards against the Altyn Tagh fault (Ritts and Biffi 2000; Cowgill *et al.* 2003; Cheng *et al.* 2015*a*, 2015*b*, 2016*b*) (Fig. 10a). Greater shortening in the west than in the east (Yin *et al.* 2008*a*; Zuza *et al.* 2016) led to broad right-lateral shear strain and net clockwise rotation against the rigid Tarim Basin and may have resulted in greater crustal thickening in the west than in the east. Progressive displacement along the Altyn Tagh fault was ultimately transferred into the fold–thrust Qilian Shan (Meyer *et al.* 1998; Searle *et al.* 2011; Cheng *et al.* 2015*b*, 2016*b*) (Fig. 10b).

As a result of progressive crustal thickening in northern Tibet, it became more mechanically efficient for strike-slip faulting to initiate at *c.* 15 Ma (Duvall *et al.* 2013; Li *et al.* 2019) along the pre-Cenozoic suture zones (Wu *et al.* 2017, 2019; Zuza *et al.* 2018*b*) and continued clockwise rotation drove left-slip bookshelf faulting of the Haiyuan and Kunlun faults (England and Molnar 1990; Zuza and Yin 2016) (Fig. 10b). The initiation of a broad left-slip transpressional system established a four-quadrant strain pattern, with fault-parallel shortening in the NW and SE quadrants and fault-parallel extension in the NE and SW quadrants. This included the activation of the right-slip Elashan and Riyeshan faults at the SW tip of the Haiyuan fault, which simultaneously accommodated fault-parallel west–east stretching and counterclockwise rotation embedded between the left-slip Kunlun and Haiyuan faults (e.g. Duvall and Clark 2010; this study). The overprinting clockwise and counterclockwise rotation led to variable net rotation that might appear negligible (Fig. 8).

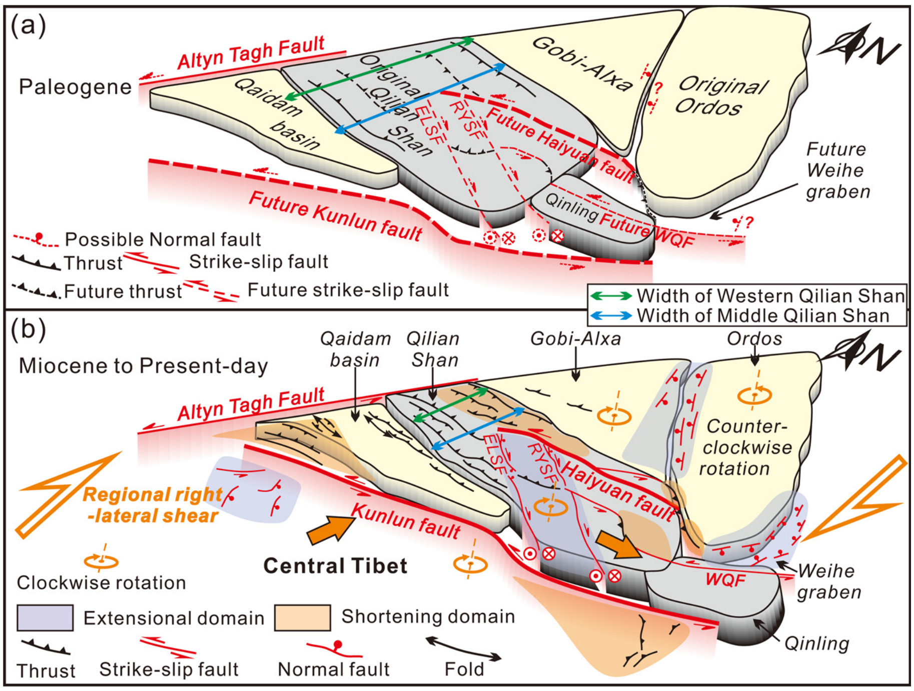

Fig 10. New hybrid model of crustal deformation in northern Tibet incorporating the eastwards displacement model (Cheng *et al.* 2015*b*) with the non-rigid passive bookshelf faulting model (Zuza and Yin 2016). Note the more significant crustal shortening in the western Qilian Shan than in the middle and eastern Qilian Shan, which indicates the eastwards migration of crustal materials in the Qilian Shan during the Cenozoic. ELSF, Elashan fault; RYSF, Riyueshan fault; WQF, Western Qinling fault. Reprinted from Cheng *et al.* 2015*b* with permission from John Wiley and Sons.

Downloaded from http://jgs.lyellcollection.org/ by GSL Maintenance User on July 7, 2021

The thicker crust and greater shortening in the west established a local stress state where eastward crustal stretching was favoured, which may be analogous to the conditions in southern Tibet (Yin *et al.* 1999; Bian *et al.* 2020). This strain condition was superimposed over the bookshelf fault kinematics outlined here and the crust between the Kunlun and Haiyuan faults extended eastwards. This explains the prevalence of normal fault structures and bulk west–east stretching (Figs 4 and 5). In this sense, progressive crustal thickening and north–south shortening in the Qilian Shan is balanced by net eastwards extrusion, as suggested by Cheng *et al.* (2015*b*). Therefore, net north-directed convergence across the Qilian Shan (Zhang *et al.* 2004; Wang and Shen 2020) is accommodated via a combination of north–south crustal shortening, tens to hundreds of kilometres of displacement along strike-slip faults, eastwards crustal stretching and clockwise rotation (Fig. 10).

As revealed by GPS and seismic anisotropy studies (Gan *et al.* 2007; Y. Li *et al.* 2011; Pan *et al.* 2020), there is a regional clockwise flow pattern across northern Tibet. Our work suggests that major strike-slip faults accommodate the continuum deformation of this region. None of these faults is a rigid block boundary, but rather they are structures of localized high strain approximating viscous flow. We acknowledge that pre-existing weaknesses throughout the Qilian Shan (e.g. suture zones) and crustal heterogeneities are reactivated as discrete faulting within this flowing body. As a result of conservation of mass requirements, this NE–SW-oriented contractional system requires NW-SE-oriented stretching, which causes the strike-slip faults to have subsidiary normal splay faults.

Conclusions

A better understanding of the geometry and kinematics of the strike-slip faults and associated structures within the Qilian Shan allows us to explore how intra-fold–thrust belt block rotation and strike-slip faulting accommodate plate convergence. We examined the Elashan and Riyueshan right-slip faults in the central Qilian Shan and our observations and slip rate constraints lead to the following conclusions.

(1) We document horsetail termination splays, discrete right-slip faults, off-fault normal faulting and releasing bends, which suggest that the right-slip faults actively accommodated block rotation and distributed west–east-oriented crustal stretching between the left-slip Haiyuan and Kunlun faults.

(2) New IRSL dating of displaced terrace risers along the Riyueshan fault provides a *c.* 1.1 mm a^{-1} slip rate estimate, similar to other published rates along this fault.

(3) The pattern of Cenozoic deformation in northern Tibet is compatible with west–east-oriented crustal stretching, non-rigid off-fault deformation and broad clockwise rotation and bookshelf faulting, which together accommodate the NE–SW-oriented India–Asia convergence.

(4) The faults in northern Tibet represent strain localization that together accommodates continuum deformation during regional clockwise lithospheric flow against the rigid Eurasian continent. Pre-existing weaknesses and strength heterogeneities cause the partitioning of deformation along dip-slip and strike-slip faults.

Acknowledgements FC and AVZ are grateful to the Chief Editor Prof. Graham Shields and Maggie Simmons and Patricia Pantos for the invitation to publish this paper. We are grateful to Editor Dr Yuntao Tian, reviewer Dr Xiubin Lin and one anonymous referee for providing insightful comments. We thank Dr Zhengyang Pan for providing the raw data for focal mechanism solutions of recent earthquakes in North Tibet.

Author contributions **FC**: conceptualization (equal), formal analysis (equal), investigation (equal), methodology (lead), visualization (lead), writing – original draft (lead); **AVZ**: conceptualization (equal), formal analysis (equal), funding acquisition (lead), investigation (equal), methodology (equal), supervision (equal), writing – review and editing (lead); **PJH**: formal analysis (equal), validation (equal), writing – review and editing (equal); **CW**: investigation (equal), validation (equal); **CN**: investigation (equal), methodology (equal), validation (equal), writing – review and editing (equal); **HC**: validation (supporting), writing – review and editing (supporting); **XL**: validation (supporting), writing – review and editing (supporting); **BL**: formal analysis (supporting), writing – review and editing (supporting).

Funding This work was funded by an open grant from the Key Laboratory of Deep-Earth Dynamics of Ministry of Natural Resource, Institute of Geology, Chinese Academy of Geological Sciences (J1901), an open grant from the State Key Laboratory of Loess and Quaternary Geology, Institute of Earth Environment, Chinese Academy of Sciences (SKLLQG1903), and a grant from the National Natural Science Foundation of China (41930213 and 41888101) to FC. The National Science Foundation (1914501), National Science Foundation (1914501) and The Tectonics Program of the National Science Foundation supported this research (EAR 1914501) with grants to AVZ and PJH. BL acknowledges grants from the Natural Science Foundation of China (U1902208) and from the Youth Innovation Promotion Association Chinese Academy of Sciences (Y201759). CN acknowledges funding from the National Science Foundation (No. 1914566) and National Natural Science Foundation of China (41888101).

Data availability All data generated or analysed during this study are included in this published article (and its supplementary information files).

Scientific editing by Yuntao Tian

References

Allen, M., Saville, C., Blanc, E., Talebian, M. and Nissen, E. 2013. Orogenic plateau growth: expansion of the Turkish–Iranian Plateau across the Zagros fold-and-thrust belt. *Tectonics*, **32**, 171–190, https://doi.org/10.1002/tect.20025

Allen, M.B., Walters, R.J. *et al.* 2017. Partitioning of oblique convergence coupled to the fault locking behavior of fold-and-thrust belts: evidence from the Qilian Shan, northeastern Tibetan Plateau. *Tectonics*, **36**, 1679–1698, https://doi.org/10.1002/2017TC004476

An, Z., Wang, P. *et al.* 2006. Geophysical survey on the tectonic and sediment distribution of Qinghai Lake basin. *Science in China Series D: Earth Sciences*, **49**, 851–861, https://doi.org/10.1007/s11430-006-0851-1

Atwater, T. 1970. Implications of plate tectonics for the Cenozoic tectonic evolution of western North America. *GSA Bulletin*, **81**, 3513–3536, https://doi.org/10.1130/0016-7606(1970)81[3513:IOPTFT]2.0.CO;2

Avouac, J.-P., Tapponnier, P., Bai, M., You, H. and Wang, G. 1993. Active thrusting and folding along the northern Tien Shan and late Cenozoic rotation of the Tarim relative to Dzungaria and Kazakhstan. *Journal of Geophysical Research: Solid Earth*, **98**, 6755–6804, https://doi.org/10.1029/92JB01963

Bartlett, W.L., Friedman, M. and Logan, J.M. 1981. Experimental folding and faulting of rocks under confining pressure. Part IX. Wrench faults in limestone layers. *Tectonophysics*, **79**, 255–277, https://doi.org/10.1016/0040-1951(81)90116-5

Bian, S., Gong, J. *et al.* 2020. Late Pliocene onset of the Cona rift, eastern Himalaya, confirms eastward propagation of extension in Himalayan–Tibetan orogen. *Earth and Planetary Science Letters*, **544**, 116383, https://doi.org/10.1016/j.epsl.2020.116383

Bovet, P.M., Ritts, B.D., Gehrels, G., Abbink, A.O., Darby, B. and Hourigan, J. 2009. Evidence of Miocene crustal shortening in the north Qilian Shan from Cenozoic stratigraphy of the western Hexi Corridor, Gansu Province, China. *American Journal of Science*, **309**, 290–329, https://doi.org/10.2475/00.4009.02

Braitenberg, C., Wang, Y., Fang, J. and Hsu, H. 2003. Spatial variations of flexure parameters over the Tibet–Quinghai plateau. *Earth and Planetary Science Letters*, **205**, 211–224, https://doi.org/10.1016/S0012-821X(02)01042-7

Burchfiel, B.C., Quidong, D., Molnar, P., Royden, L., Yipeng, W., Peizhen, Z. and Weiqi, Z. 1989. Intracrustal detachment within zones of continental deformation. *Geology*, **17**, 748–752, https://doi.org/10.1130/0091-7613(1989)017<0448:IDWZOC>2.3.CO;2

Burchfiel, B., Zhang, P. *et al.* 1991. Geology of the Haiyuan fault zone, Ningxia-Hui Autonomous Region, China, and its relation to the evolution of the northeastern margin of the Tibetan Plateau. *Tectonics*, **10**, 1091–1110, https://doi.org/10.1029/90TC02685

Champagnac, J.-D., Yuan, D.-Y., Ge, W.-P., Molnar, P. and Zheng, W.-J. 2010. Slip rate at the north-eastern front of the Qilian Shan, China. *Terra Nova*, **22**, 180–187, https://doi.org/10.1111/j.1365-3121.2010.00932.x

Chen, P. and Lin, A. 2019. Tectonic topography and Late Pleistocene activity of the West Qinling Fault, northeastern Tibetan Plateau. *Journal of Asian Earth Sciences*, **176**, 68–78, https://doi.org/10.1016/j.jseaes.2019.02.007

Chen, W.-P. and Molnar, P. 1983. Focal depths of intracontinental and intraplate earthquakes and their implications for the thermal and mechanical properties

Downloaded from http://jgs.lyellcollection.org/ by GSL Maintenance User on July 7, 2021

of the lithosphere. *Journal of Geophysical Research: Solid Earth*, **88**, 4183–4214, https://doi.org/10.1029/JB088iB05p04183
Chen, Y., Gilder, S., Halim, N., Cogné, J.P. and Courtillot, V. 2002. New paleomagnetic constraints on central Asian kinematics: displacement along the Altyn Tagh fault and rotation of the Qaidam Basin. *Tectonics*, **21**, 1042, https://doi.org/10.1029/2001TC901030
Cheng, F., Jolivet, M., Fu, S., Zhang, Q., Guan, S., Yu, X. and Guo, Z. 2014. Northward growth of the Qimen Tagh range: a new model accounting for the Late Neogene strike-slip deformation of the SW Qaidam Basin. *Tectonophysics*, **632**, 32–47, https://doi.org/10.1016/j.tecto.2014.05.034
Cheng, F., Guo, Z., Jenkins, H.S., Fu, S. and Cheng, X. 2015*a*. Initial rupture and displacement on the Altyn Tagh fault, northern Tibetan Plateau: constraints based on residual Mesozoic to Cenozoic strata in the western Qaidam Basin. *Geosphere*, **11**, 921–942, https://doi.org/10.1130/GES01070.1
Cheng, F., Jolivet, M., Dupont-Nivet, G., Wang, L., Yu, X. and Guo, Z. 2015*b*. Lateral extrusion along the Altyn Tagh Fault, Qilian Shan (NE Tibet): insight from a 3D crustal budget. *Terra Nova*, **27**, 416–425, https://doi.org/10.1111/ter.12173
Cheng, F., Fu, S., Jolivet, M., Zhang, C. and Guo, Z. 2016*a*. Source to sink relation between the Eastern Kunlun Range and the Qaidam Basin, northern Tibetan Plateau, during the Cenozoic. *GSA Bulletin*, **128**, 258–283, https://doi.org/10.1130/B31260.1
Cheng, F., Jolivet, M., Fu, S., Zhang, C., Zhang, Q. and Guo, Z. 2016*b*. Large-scale displacement along the Altyn Tagh Fault (North Tibet) since its Eocene initiation: insight from detrital zircon U–Pb geochronology and subsurface data. *Tectonophysics*, **677–678**, 261–279, https://doi.org/10.1016/j.tecto.2016.04.023
Cheng, F., Jolivet, M., Hallot, E., Zhang, D., Zhang, C. and Guo, Z. 2017. Tectono-magmatic rejuvenation of the Qaidam craton, northern Tibet. *Gondwana Research*, **49**, 248–263, https://doi.org/10.1016/j.gr.2017.06.004
Cheng, F., Garzione, C., Jolivet, M., Wang, W., Dong, J., Richter, F. and Guo, Z. 2019*a*. Provenance analysis of the Yumen Basin and northern Qilian Shan: implications for the pre-collisional paleogeography in the NE Tibetan Plateau and eastern termination of Altyn Tagh fault. *Gondwana Research*, **65**, 156–171, https://doi.org/10.1016/j.gr.2018.08.009
Cheng, F., Garzione, C.N. *et al.* 2019*b*. The interplay between climate and tectonics during the upward and outward growth of the Qilian Shan orogenic wedge, northern Tibetan Plateau. *Earth-Science Reviews*, **198**, 102945, https://doi.org/10.1016/j.earscirev.2019.102945
Cheng, F., Jolivet, M. *et al.* 2019*c*. Jurassic–Early Cenozoic tectonic inversion in the Qilian Shan and Qaidam Basin, North Tibet: new insight from seismic reflection, isopach mapping, and drill core data. *Journal of Geophysical Research: Solid Earth*, **124**, 12077–12098, https://doi.org/10.1029/2019JB018086
Cobbold, P. and Davy, P. 1988. Indentation tectonics in nature and experiment. 2. Central Asia. *Bulletin of the Geological Institute of the University of Uppsala*, **14**, 143–162.
Cogné, J.P., Halim, N., Chen, Y. and Courtillot, V. 1999. Resolving the problem of shallow magnetizations of Tertiary age in Asia: insights from paleomagnetic data from the Qiangtang, Kunlun, and Qaidam blocks (Tibet, China), and a new hypothesis. *Journal of Geophysical Research: Solid Earth*, **104**, 17715–17734, https://doi.org/10.1029/1999JB900153
Cowgill, E. 2007. Impact of riser reconstructions on estimation of secular variation in rates of strike–slip faulting: revisiting the Cherchen River site along the Altyn Tagh Fault, NW China. *Earth and Planetary Science Letters*, **254**, 239–255, https://doi.org/10.1016/j.epsl.2006.09.015
Cowgill, E., Yin, A., Harrison, T.M. and Xiao-Feng, W. 2003. Reconstruction of the Altyn Tagh fault based on U-Pb geochronology: role of back thrusts, mantle sutures, and heterogeneous crustal strength in forming the Tibetan Plateau. *Journal of Geophysical Research*, **108**, 2346, https://doi.org/10.1029/2002JB002080
Craddock, W., Kirby, E. and Zhang, H. 2011. Late Miocene–Pliocene range growth in the interior of the northeastern Tibetan Plateau. *Lithosphere*, **3**, 420–438, https://doi.org/10.1130/L159.1
Cunningham, W.D. and Mann, P. 2007. Tectonics of strike-slip restraining and releasing bends. *Geological Society, London, Special Publications*, **290**, 1–12, https://doi.org/10.1144/SP290.1
Davis, G.A. and Burchfiel, B.C. 1973. Garlock Fault: an intracontinental transform structure, southern California. *GSA Bulletin*, **84**, 1407–1422, https://doi.org/10.1130/0016-7606(1973)84<1407:GFAITS>2.0.CO;2.
Davis, G.H., Bump, A.P., García, P.E. and Ahlgren, S.G. 2000. Conjugate Riedel deformation band shear zones. *Journal of Structural Geology*, **22**, 169–190, https://doi.org/10.1016/S0191-8141(99)00140-6
Dewey, J.F. and Burke, K.C. 1973. Tibetan, Variscan, and Precambrian basement reactivation: products of continental collision. *The Journal of Geology*, **81**, 683–692, https://doi.org/10.1086/627920
Ding, G., Chen, J., Tian, Q., Shen, X., Xing, C. and Wei, K. 2004. Active faults and magnitudes of left-lateral displacement along the northern margin of the Tibetan Plateau. *Tectonophysics*, **380**, 243–260, https://doi.org/10.1016/j.tecto.2003.09.022
Dupont-Nivet, G., Butler, R.F., Yin, A. and Chen, X. 2002. Paleomagnetism indicates no Neogene rotation of the Qaidam Basin in northern Tibet during Indo-Asian collision. *Geology*, **30**, 263–266, https://doi.org/10.1130/0091-7613(2002)030<0263:PINNRO>2.0.CO;2
Dupont-Nivet, G., Butler, R.F., Yin, A. and Chen, X. 2003. Paleomagnetism indicates no Neogene vertical axis rotations of the northeastern Tibetan Plateau. *Journal of Geophysical Research*, **108**, 2386, https://doi.org/10.1029/2003JB002399
Duvall, A.R. and Clark, M.K. 2010. Dissipation of fast strike-slip faulting within and beyond northeastern Tibet. *Geology*, **38**, 223–226, https://doi.org/10.1130/G30711.1
Duvall, A.R., Clark, M.K., Kirby, E., Farley, K.A., Craddock, W.H., Li, C. and Yuan, D.-Y. 2013. Low-temperature thermochronometry along the Kunlun and Haiyuan Faults, NE Tibetan Plateau: evidence for kinematic change during late-stage orogenesis. *Tectonics*, **32**, 1190–1211, https://doi.org/10.1002/tect.20072
Elliott, A.J., Oskin, M.E., Liu-zeng, J. and Shao, Y.X. 2018. Persistent rupture terminations at a restraining bend from slip rates on the eastern Altyn Tagh fault. *Tectonophysics*, **733**, 57–72, https://doi.org/10.1016/j.tecto.2018.01.004
England, P. and Houseman, G. 1986. Finite strain calculations of continental deformation: 2. Comparison with the India–Asia collision zone. *Journal of Geophysical Research: Solid Earth*, **91**, 3664–3676, https://doi.org/10.1029/JB091iB03p03664
England, P. and Molnar, P. 1990. Surface uplift, uplift of rocks, and exhumation of rocks. *Geology*, **18**, 1173–1177, https://doi.org/10.1130/0091-7613(1990)018<1173:SUUORA>2.3.CO;2
Evans, E.L., Thatcher, W.R., Pollitz, F.F. and Murray, J.R. 2016. Persistent slip rate discrepancies in the eastern California (USA) shear zone. *Geology*, **44**, 691–694, https://doi.org/10.1130/G37967.1
Fang, X., Garzione, C., Van der Voo, R., Li, J. and Fan, M. 2003. Flexural subsidence by 29 Ma on the NE edge of Tibet from the magnetostratigraphy of Linxia Basin, China. *Earth and Planetary Science Letters*, **210**, 545–560, https://doi.org/10.1016/S0012-821X(03)00142-0
Flesch, L.M., Holt, W.E., Haines, A.J. and Shen-Tu, B. 2000. Dynamics of the Pacific–North American plate boundary in the western United States. *Science*, **287**, 834—836, https://doi.org/10.1126/science.287.5454.834
Fu, C., An, Z., Qiang, X., Bloemendal, J., Song, Y. and Chang, H. 2013. Magnetostratigraphic determination of the age of ancient Lake Qinghai, and record of the East Asian monsoon since 4.63 Ma. *Geology*, **41**, 875–878, https://doi.org/10.1130/G34418.1
Galbraith, R.F., Roberts, R.G., Laslett, G.M., Yoshida, H. and Olley, J.M. 1999. Optical dating of single and multiple grains of quartz from Jinmium rock shelter, northern Australia: part I, experimental design and statistical models. *Archaeometry*, **41**, 339–364, https://doi.org/10.1111/j.1475-4754.1999.tb00987.x
Gan, W., Zhang, P. *et al.* 2007. Present-day crustal motion within the Tibetan Plateau inferred from GPS measurements. *Journal of Geophysical Research: Solid Earth*, **112**, B08416, https://doi.org/10.1029/2005JB004120.
Gaudemer, Y., Tapponnier, P. *et al.* 1995. Partitioning of crustal slip between linked, active faults in the eastern Qilian Shan, and evidence for a major seismic gap, the 'Tianzhu gap', on the western Haiyuan Fault, Gansu (China). *Geophysical Journal International*, **120**, 599–645, https://doi.org/10.1111/j.1365-246X.1995.tb01842.x
George, A.D., Marshallsea, S.J., Wyrwoll, K.-H., Jie, C. and Yanchou, L. 2001. Miocene cooling in the northern Qilian Shan, northeastern margin of the Tibetan Plateau, revealed by apatite fission-track and vitrinite-reflectance analysis. *Geology*, **29**, 939–942, https://doi.org/10.1130/0091-7613(2001)029<0939:MCITNQ>2.0.CO;2
Ghosh, A., Holt, W.E., Flesch, L.M. and Haines, A.J. 2006. Gravitational potential energy of the Tibetan Plateau and the forces driving the Indian plate. *Geology*, **34**, 321–324, https://doi.org/10.1130/G22071.1
Gold, R.D., Cowgill, E., Arrowsmith, J.R. and Friedrich, A.M. 2017. Pulsed strain release on the Altyn Tagh fault, northwest China. *Earth and Planetary Science Letters*, **459**, 291–300, https://doi.org/10.1016/j.epsl.2016.11.024
Guo, Z.J., Yin, A., Robinson, A. and Jia, C.Z. 2005. Geochronology and geochemistry of deep-drill-core samples from the basement of the central Tarim basin. *Journal of Asian Earth Sciences*, **25**, 45–56, https://doi.org/10.1016/j.jseaes.2004.01.016
Halim, N., Chen, Y. and Cogné, J. 2003. A first palaeomagnetic study of Jurassic formations from the Qaidam basin, northeastern Tibet, China—tectonic implications. *Geophysical Journal International*, **153**, 20–26, https://doi.org/10.1046/j.1365-246X.2003.01860.x
Haproff, P.J., Zuza, A.V. and Yin, A. 2018. West-directed thrusting south of the eastern Himalayan syntaxis indicates clockwise crustal flow at the indenter corner during the India–Asia collision. *Tectonophysics*, **722**, 277–285, https://doi.org/10.1016/j.tecto.2017.11.001
Harkins, N. and Kirby, E. 2008. Fluvial terrace riser degradation and determination of slip rates on strike-slip faults: an example from the Kunlun fault, China. *Geophysical Research Letters*, **35**, L05406, https://doi.org/10.1029/2007GL033073
Harkins, N., Kirby, E., Shi, X., Wang, E., Burbank, D. and Chun, F. 2010. Millennial slip rates along the eastern Kunlun fault: implications for the dynamics of intracontinental deformation in Asia. *Lithosphere*, **2**, 247–266, https://doi.org/10.1130/L85.1
He, P., Song, C., Wang, Y., Chen, L., Chang, P., Wang, Q. and Ren, B. 2017. Cenozoic exhumation in the Qilian Shan, northeastern Tibetan Plateau: evidence from detrital fission track thermochronology in the Jiuquan Basin.

Downloaded from http://jgs.lyellcollection.org/ by GSL Maintenance User on July 7, 2021

Journal of Geophysical Research: Solid Earth, **122**, 6910–6927, https://doi.org/10.1002/2017JB014216

He, P., Song, C. *et al.* 2018. Cenozoic deformation history of the Qilian Shan (northeastern Tibetan Plateau) constrained by detrital apatite fission-track thermochronology in the northeastern Qaidam Basin. *Tectonophysics*, **749**, 1–11, https://doi.org/10.1016/j.tecto.2018.10.017

Hetzel, R., Niedermann, S., Tao, M., Kubik, P.W., Ivy-Ochs, S., Gao, B. and Strecker, M.R. 2002. Low slip rates and long-term preservation of geomorphic features in Central Asia. *Nature*, **417**, 428–432, https://doi.org/10.1038/417428a

Huang, H., Niu, Y., Nowell, G., Zhao, Z., Yu, X. and Mo, X. 2015. The nature and history of the Qilian Block in the context of the development of the Greater Tibetan Plateau. *Gondwana Research*, **28**, 209–224, https://doi.org/10.1016/j.gr.2014.02.010

Hubbard, J. and Shaw, J.H. 2009. Uplift of the Longmen Shan and Tibetan Plateau, and the 2008 Wenchuan ($M = 7.9$) earthquake. *Nature*, **458**, 194–197, https://doi.org/10.1038/nature07837

Huntley, D.J. and Lamothe, M. 2001. Ubiquity of anomalous fading in K-feldspars and the measurement and correction for it in optical dating. *Canadian Journal of Earth Sciences*, **38**, 1093–1106, https://doi.org/10.1139/e01-013

Jiang, W., Han, Z., Guo, P., Zhang, J., Jiao, Q., Kang, S. and Tian, Y. 2017. Slip rate and recurrence intervals of the east Lenglongling fault constrained by morphotectonics: tectonic implications for the northeastern Tibetan Plateau. *Lithosphere*, **9**, 417–430, https://doi.org/10.1130/L597.1%J Lithosphere

Johnson, K.M. 2013. Slip rates and off-fault deformation in southern California inferred from GPS data and models. *Journal of Geophysical Research: Solid Earth*, **118**, 5643–5664, https://doi.org/10.1002/jgrb.50365

Jolivet, M., Brunel, M. *et al.* 2001. Mesozoic and Cenozoic tectonics of the northern edge of the Tibetan Plateau: fission-track constraints. *Tectonophysics*, **343**, 111–134, https://doi.org/10.1016/S0040-1951(01)00196-2

Jolivet, M., Brunel, M. *et al.* 2003. Neogene extension and volcanism in the Kunlun Fault Zone, northern Tibet: new constraints on the age of the Kunlun Fault. *Tectonics*, **22**, 1052, https://doi.org/10.1029/2002TC001428

Kirby, E., Harkins, N., Wang, E., Shi, X., Fan, C. and Burbank, D. 2007. Slip rate gradients along the eastern Kunlun fault. *Tectonics*, **26**, TC2010, https://doi.org/10.1029/2006TC002033

Kusky, T. and Mooney, W. 2015. Is the Ordos Basin floored by a trapped oceanic plateau? *Earth and Planetary Science Letters*, **429**, 197–204, https://doi.org/10.1016/j.epsl.2015.07.069

Lasserre, C., Morel, P.H. *et al.* 1999. Postglacial left slip rate and past occurrence of $M \geq 8$ earthquakes on the western Haiyuan fault, Gansu, China. *Journal of Geophysical Research: Solid Earth*, **104**, 17633–17651, https://doi.org/10.1029/1998JB900082

Lasserre, C., Gaudemer, Y. *et al.* 2002. Fast late Pleistocene slip rate on the Leng Long Ling segment of the Haiyuan fault, Qinghai, China. *Journal of Geophysical Research: Solid Earth*, **107**, ETG 4-1-ETG 4-15, 2276, https://doi.org/10.1029/2000JB000060.

Lease, R.O. 2014. Cenozoic mountain building on the northeastern Tibetan Plateau. *Geological Society of America, Special Papers*, **507**, 115–127, https://doi.org/10.1130/2014.2507(06)

Lease, R.O., Burbank, D.W., Clark, M.K., Farley, K.A., Zheng, D. and Zhang, H. 2011. Middle Miocene reorganization of deformation along the northeastern Tibetan Plateau. *Geology*, **39**, 359–362, https://doi.org/10.1130/G31356.1

Li, B., Chen, X., Zuza, A.V., Hu, D., Ding, W., Huang, P. and Xu, S. 2019. Cenozoic cooling history of the North Qilian Shan, northern Tibetan Plateau, and the initiation of the Haiyuan fault: constraints from apatite- and zircon-fission track thermochronology. *Tectonophysics*, **751**, 109–124, https://doi.org/10.1016/j.tecto.2018.12.005

Li, B., Zuza, A.V. *et al.* 2020*a*. Pre-Cenozoic evolution of the northern Qilian Orogen from zircon geochronology: framework for early growth of the northern Tibetan Plateau. *Palaeogeography, Palaeoclimatology, Palaeoecology*, **562**, 110091, https://doi.org/10.1016/j.palaeo.2020.110091

Li, B., Zuza, A.V. *et al.* 2020*b*. Cenozoic multi-phase deformation in the Qilian Shan and out-of-sequence development of the northern Tibetan Plateau. *Tectonophysics*, **782–783**, 228423, https://doi.org/10.1016/j.tecto.2020.228423

Li, C., Zhang, P.-Z., Yin, J. and Min, W. 2009. Late Quaternary left-lateral slip rate of the Haiyuan fault, northeastern margin of the Tibetan Plateau. *Tectonics*, **28**, https://doi.org/10.1029/2008TC002302

Li, C., Xu, X. *et al.* 2011. Rupture segmentation and slip partitioning of the mid-eastern part of the Kunlun Fault, north Tibetan Plateau. *Science China Earth Sciences*, **54**, 1730–1745, https://doi.org/10.1007/s11430-011-4239-5

Li, H., Van der Woerd, J., Tapponnier, P., Klinger, Y., Qi, X., Yang, J. and Zhu, Y. 2005. Slip rate on the Kunlun fault at Hongshui Gou, and recurrence time of great events comparable to the 14/11/2001, Mw∼7.9 Kokoxili earthquake. *Earth and Planetary Science Letters*, **237**, 285–299, https://doi.org/10.1016/j.epsl.2005.05.041

Li, Y., Wu, Q., Zhang, F., Feng, Q. and Zhang, R. 2011. Seismic anisotropy of the northeastern Tibetan Plateau from shear wave splitting analysis. *Earth and Planetary Science Letters*, **304**, 147–157, https://doi.org/10.1016/j.epsl.2011.01.026

Lin, A. and Guo, J. 2008. Nonuniform slip rate and millennial recurrence interval of large earthquakes along the eastern segment of the Kunlun Fault, northern Tibet. *Bulletin of the Seismological Society of America*, **98**, 2866–2878, https://doi.org/10.1785/0120070193

Lin, A., Guo, J., Kano, K.-i. and Awata, Y. 2006. Average slip rate and recurrence interval of large-magnitude earthquakes on the western segment of the strike-slip Kunlun Fault, northern Tibet. *Bulletin of the Seismological Society of America*, **96**, 1597–1611, https://doi.org/10.1785/0120050051

Lin, X., Chen, H., Wyrwoll, K.-H., Batt, G.E., Liao, L. and Xiao, J. 2011. The uplift history of the Haiyuan-Liupan Shan region northeast of the present Tibetan Plateau: integrated constraint from stratigraphy and thermochronology. *The Journal of Geology*, **119**, 372–393, https://doi.org/10.1086/660190

Liritzis, I., Stamoulis, K., Papachristodoulou, C. and Ioannides, K. 2013. A re-evaluation of radiation dose-rate conversion factors. *Mediterranean Archaeology Archaeometry*, **13**, 1–15.

Liu, Z., Zhao, X., Wang, C., Liu, S. and Yi, H. 2003. Magnetostratigraphy of Tertiary sediments from the Hoh Xil Basin: implications for the Cenozoic tectonic history of the Tibetan Plateau. *Geophysical Journal International*, **154**, 233–252, https://doi.org/10.1046/j.1365-246X.2003.01986.x

Liu-Zeng, J., Klinger, Y. *et al.* 2007. Millennial recurrence of large earthquakes on the Haiyuan Fault near Songshan, Gansu Province, China. *Bulletin of the Seismological Society of America*, **97**, 14–34, https://doi.org/10.1785/0120050118

Luo, H., He, W., Yuan, D. and Shao, Y. 2015. Slip rate of Yema River–Daxue Mountain Fault since the Late Pleistocene and its implications on the deformation of the northeastern margin of the Tibetan Plateau. *Acta Geologica Sinica (English Edition,)*, **89**, 561–574, https://doi.org/10.1111/1755-6724.12447

Luyendyk, B.P., Kamerling, M.J. and Terres, R. 1980. Geometric model for Neogene crustal rotations in southern California. *GSA Bulletin*, **91**, 211–217, https://doi.org/10.1130/0016-7606(1980)91<211:GMFNCR>2.0.CO;2

Matrau, R., Klinger, Y., Van der Woerd, J., Liu-Zeng, J., Li, Z., Xu, X. and Zheng, R. 2019. Late Pleistocene–Holocene slip rate along the Hasi Shan restraining bend of the Haiyuan Fault: implication for faulting dynamics of a complex fault system. *Tectonics*, **38**, 4127–4154, https://doi.org/10.1029/2019TC005488

Meade, B.J. 2007. Present-day kinematics at the India–Asia collision zone. *Geology*, **35**, 81–84, https://doi.org/10.1130/G22924A.1

Meade, B.J. and Hager, B.H. 2005. Block models of crustal motion in southern California constrained by GPS measurements. *Journal of Geophysical Research: Solid Earth*, **110**, https://doi.org/10.1029/2004JB003209

Métivier, F., Gaudemer, Y., Tapponnier, P. and Meyer, B. 1998. Northeastward growth of the Tibet Plateau deduced from balanced reconstruction of two depositional areas: the Qaidam and Hexi Corridor basins, China. *Tectonics*, **17**, 823–842, https://doi.org/10.1029/98TC02764

Meyer, B., Tapponnier, P. *et al.* 1998. Crustal thickening in Gansu-Qinghai, lithospheric mantle subduction, and oblique, strike-slip controlled growth of the Tibet Plateau. *Geophysical Journal International*, **135**, 1–47, https://doi.org/10.1046/j.1365-246X.1998.00567.x

Molnar, P. and Tapponnier, P. 1975. Cenozoic tectonics of Asia: effects of a continental collision. *Science*, **189**, 419–426, https://doi.org/10.1126/science.189.4201.419

Mouthereau, F., Watts, A.B. and Burov, E. 2013. Structure of orogenic belts controlled by lithosphere age. *Nature Geoscience*, **6**, 785–789, https://doi.org/10.1038/ngeo1902

Murphy, M., Yin, A. *et al.* 1997. Did the Indo-Asian collision alone create the Tibetan Plateau? *Geology*, **25**, 719–722, https://doi.org/10.1130/0091-7613(1997)025<0719:DTIACA>2.3.CO;2

Pan, Z., He, J. and Shao, Z. 2020. Spatial variation in the present-day stress field and tectonic regime of northeast Tibet from moment tensor solutions of local earthquake data. *Geophysical Journal International*, **221**, 478–491, https://doi.org/10.1093/gji/ggaa013

Platt, J.P. and Becker, T.W. 2010. Where is the real transform boundary in California? *Geochemistry, Geophysics, Geosystems*, **11**, Q06012, https://doi.org/10.1029/2010GC003060

Platt, J.P. and Becker, T.W. 2013. Kinematics of rotating panels of E–W faults in the San Andreas system: what can we tell from geodesy? *Geophysical Journal International*, **194**, 1295–1301, https://doi.org/10.1093/gji/ggt189

Prescott, J.R. and Hutton, J.T. 1994. Cosmic ray contributions to dose rates for luminescence and ESR dating: large depths and long-term time variations. *Radiation Measurements*, **23**, 497–500, https://doi.org/10.1016/1350-4487(94)90086-8

Pullen, A., Kapp, P., Gehrels, G.E., Vervoort, J.D. and Ding, L. 2008. Triassic continental subduction in central Tibet and Mediterranean-style closure of the Paleo-Tethys Ocean. *Geology*, **36**, 351–354, https://doi.org/10.1130/G24435A.1

Qinghai-Geology-Bureau 1976. *Regional Geological Surveying Report of the People's Republic of China: Kuairima Area (1:200, 000)*. Qinghai Geology Bureau.

Ren, J., Xu, X., Zhang, S., Ding, R., Liu, H., Liang, O. and Zhao, J. 2019. Late Quaternary slip rates and Holocene paleoearthquakes of the eastern Yumu Shan fault, northeast Tibet: implications for kinematic mechanism and seismic hazard. *Journal of Asian Earth Sciences*, **176**, 42–56, https://doi.org/10.1016/j.jseaes.2019.02.006

Ritts, B.D. and Biffi, U. 2000. Magnitude of post-Middle Jurassic (Bajocian) displacement on the central Altyn Tagh fault system, northwest China. *GSA Bulletin*, **112**, 61–74, https://doi.org/10.1130/0016-7606(2000)112<61:MOPJBD>2.0.CO;2

Downloaded from http://jgs.lyellcollection.org/ by GSL Maintenance User on July 7, 2021

Ryan, W.B.F., Carbotte, S.M. *et al.* 2009. Global multi-resolution topography synthesis. *Geochemistry, Geophysics, Geosystems*, **10**, Q03014, https://doi.org/10.1029/2008GC002332

Searle, M., Elliott, J., Phillips, R. and Chung, S.-L. 2011. Crustal–lithospheric structure and continental extrusion of Tibet. *Journal of the Geological Society, London*, **168**, 633–672, https://doi.org/10.1144/0016-76492010-139

Shao, Y., Liu-Zeng, J. *et al.* 2020. Late Pleistocene slip rate of the central Haiyuan fault constrained from optically stimulated luminescence, ^{14}C, and cosmogenic isotope dating and high-resolution topography. *GSA Bulletin*, https://doi.org/10.1130/B35571.1.

Shen, X., Tian, Y. *et al.* 2019. Late Miocene hinterland crustal shortening in the Longmen Shan thrust belt, the eastern margin of the Tibetan Plateau. *Journal of Geophysical Research: Solid Earth*, **124**, 11972–11991, https://doi.org/10.1029/2019JB018358

Song, S., Niu, Y., Zhang, L., Wei, C., Liou, J.G. and Su, L. 2009. Tectonic evolution of early Paleozoic HP metamorphic rocks in the North Qilian Mountains, NW China: new perspectives. *Journal of Asian Earth Sciences*, **35**, 334–353, https://doi.org/10.1016/j.jseaes.2008.11.005

Song, S., Su, L., Li, X.-H., Niu, Y. and Zhang, L. 2012. Grenville-age orogenesis in the Qaidam-Qilian block: the link between South China and Tarim. *Precambrian Research*, **220**, 9–22, https://doi.org/10.1016/j.precamres.2012.07.007

Song, S., Niu, Y., Su, L. and Xia, X. 2013. Tectonics of the North Qilian orogen, NW China. *Gondwana Research*, **23**, 1378–1401, https://doi.org/10.1016/j.gr.2012.02.004

Tapponnier, P., Peltzer, G., Armijo, R. and Cobbold, P. 1982. Propagating extrusion tectonics in Asia; new insights from simple experiments with plasticine. *Geology*, **10**, 611–616, https://doi.org/10.1130/0091-7613(1982)10<611:PETIAN>2.0.CO;2

Tapponnier, P., Meyer, B. *et al.* 1990. Active thrusting and folding in the Qilian Shan, and decoupling between upper crust and mantle in northeastern Tibet. *Earth and Planetary Science Letters*, **97**, 382–403, https://doi.org/10.1016/0012-821X(90)90053-Z

Taylor, M. and Yin, A. 2009. Active structures of the Himalayan–Tibetan orogen and their relationships to earthquake distribution, contemporary strain field, and Cenozoic volcanism. *Geosphere*, **5**, 199–214, https://doi.org/10.1130/GES00217.1

Thatcher, W., Savage, J.C. and Simpson, R.W. 2016. The Eastern California Shear Zone as the northward extension of the southern San Andreas Fault. *Journal of Geophysical Research: Solid Earth*, **121**, 2904–2914, https://doi.org/10.1002/2015JB012678

Tian, Y., Kohn, B.P., Phillips, D., Hu, S., Gleadow, A.J. and Carter, A. 2016. Late Cretaceous–earliest Paleogene deformation in the Longmen Shan fold-and-thrust belt, eastern Tibetan Plateau margin: pre-Cenozoic thickened crust? *Tectonics*, **35**, 2293–2312, https://doi.org/10.1002/2016TC004182

Tung, K., Yang, H.-J., Yang, H.-Y., Liu, D., Zhang, J., Wan, Y. and Tseng, C.-Y. 2007. SHRIMP U–Pb geochronology of the zircons from the Precambrian basement of the Qilian Block and its geological significances. *Chinese Science Bulletin*, **52**, 2687–2701, https://doi.org/10.1007/s11434-007-0356-0

Tung, K.-A., Yang, H.-Y., Liu, D.-Y., Zhang, J.-X., Yang, H.-J., Shau, Y.-H. and Tseng, C.-Y. 2013. The Neoproterozoic granitoids from the Qilian block, NW China: evidence for a link between the Qilian and South China blocks. *Precambrian Research*, **235**, 163–189, https://doi.org/10.1016/j.precamres.2013.06.016

Van Der Woerd, J., Ryerson, F.J. *et al.* 1998. Holocene left-slip rate determined by cosmogenic surface dating on the Xidatan segment of the Kunlun fault (Qinghai, China). *Geology*, **26**, 695–698, https://doi.org/10.1130/0091-7613(1998)026<0695:HLSRDB>2.3.CO;2

Van Der Woerd, J., Ryerson, F.J. *et al.* 2000. Uniform slip-rate along the Kunlun Fault: implications for seismic behaviour and large-scale tectonics. *Geophysical Research Letters*, **27**, 2353–2356, https://doi.org/10.1029/1999GL011292

Van Der Woerd, J., Tapponnier, P. *et al.* 2002. Uniform postglacial slip-rate along the central 600 km of the Kunlun Fault (Tibet), from ^{26}Al, ^{10}Be, and ^{14}C dating of riser offsets, and climatic origin of the regional morphology. *Geophysical Journal International*, **148**, 356–388, https://doi.org/10.1046/j.1365-246x.2002.01556.x

Wan, Y.S., Xu, Z.Q., Yang, J.S. and Zhang, J.X. 2001. Ages and compositions of the Precambrian high-grade basement of the Qilian Terrane and its adjacent areas. *Acta Geologica Sinica (English Edition)*, **75**, 375–384, https://doi.org/10.1111/j.1755-6724.2001.tb00055.x.

Wang, C., Li, R.-S., Smithies, R.H., Li, M., Peng, Y., Chen, F.-N. and He, S.-P. 2017. Early Paleozoic felsic magmatic evolution of the western Central Qilian belt, northwestern China, and constraints on convergent margin processes. *Gondwana Research*, **41**, 301–324, https://doi.org/10.1016/j.gr.2015.12.009

Wang, C.S., Gao, R. *et al.* 2011. A mid-crustal strain-transfer model for continental deformation: a new perspective from high-resolution deep seismic-reflection profiling across NE Tibet. *Earth and Planetary Science Letters*, **306**, 279–288, https://doi.org/10.1016/j.epsl.2011.04.010

Wang, E. and Burchfiel, B.C. 1997. Interpretation of Cenozoic tectonics in the right-lateral accommodation zone between the Ailao Shan Shear Zone and the Eastern Himalayan syntaxis. *International Geology Review*, **39**, 191–219, https://doi.org/10.1080/00206819709465267

Wang, E., Xu, F.-Y., Zhou, J.-X., Wan, J. and Burchfiel, B.C. 2006. Eastward migration of the Qaidam basin and its implications for Cenozoic evolution of the Altyn Tagh fault and associated river systems. *GSA Bulletin*, **118**, 349–365, https://doi.org/10.1130/B25778.1

Wang, L., MacLennan, S.A. and Cheng, F. 2020. From a proximal-deposition-dominated basin sink to a significant sediment source to the Chinese Loess Plateau: insight from the quantitative provenance analysis on the Cenozoic sediments in the Qaidam basin, northern Tibetan Plateau. *Palaeogeography, Palaeoclimatology, Palaeoecology*, **556**, 109883, https://doi.org/10.1016/j.palaeo.2020.109883

Wang, M. and Shen, Z.-K. 2020. Present-day crustal deformation of continental China derived from GPS and its tectonic implications. *Journal of Geophysical Research: Solid Earth*, **125**, e2019JB018774, https://doi.org/10.1029/2019JB018774.

Wang, T., Wang, Z., Yan, Z., Ma, Z., He, S., Fu, C. and Wang, D. 2016. Geochronological and geochemical evidence of amphibolite from the Hualong Group, northwest China: implication for the early Paleozoic accretionary tectonics of the Central Qilian belt. *Lithos*, **248**, 12–21, https://doi.org/10.1016/j.lithos.2016.01.012

Wang, W., Zhang, P. *et al.* 2016. The Cenozoic growth of the Qilian Shan in the northeastern Tibetan Plateau: a sedimentary archive from the Jiuxi Basin. *Journal of Geophysical Research: Solid Earth*, **121**, 2235–2257, https://doi.org/10.1002/2015JB012689

Wang, W.-T., Zhang, P.-Z., Kirby, E., Wang, L.-H., Zhang, G.-L., Zheng, D.-W. and Chai, C.-Z. 2011. A revised chronology for Tertiary sedimentation in the Sikouzi basin: implications for the tectonic evolution of the northeastern corner of the Tibetan Plateau. *Tectonophysics*, **505**, 100–114, https://doi.org/10.1016/j.tecto.2011.04.006

Wang, X., Zattin, M., Li, J., Song, C., Peng, T., Liu, S. and Liu, B. 2011. Eocene to Pliocene exhumation history of the Tianshui–Huicheng region determined by apatite fission track thermochronology: implications for evolution of the northeastern Tibetan Plateau margin. *Journal of Asian Earth Sciences*, **42**, 97–110, https://doi.org/10.1016/j.jseaes.2011.04.012

Weldon, R. and Humphreys, E. 1986. A Kinematic model of southern California. *Tectonics*, **5**, 33–48, https://doi.org/10.1029/TC005i001p00033

Wu, C., Yin, A., Zuza, A.V., Zhang, J., Liu, W. and Ding, L. 2016. Pre-Cenozoic geologic history of the central and northern Tibetan Plateau and the role of Wilson cycles in constructing the Tethyan orogenic system. *Lithosphere*, **8**, 254–292, https://doi.org/10.1130/L494.1

Wu, C., Zuza, A.V. *et al.* 2017. Geochronology and geochemistry of Neoproterozoic granitoids in the central Qilian Shan of northern Tibet: reconstructing the amalgamation processes and tectonic history of Asia. *Lithosphere*, **9**, 609–636, https://doi.org/10.1130/L640.1

Wu, C., Zuza, A.V. *et al.* 2019. Tectonics of the Eastern Kunlun Range: Cenozoic reactivation of a Paleozoic–Early Mesozoic Orogen. *Tectonics*, **38**, 1609–1650, https://doi.org/10.1029/2018TC005370

Xiao, W., Windley, B.F., Yong, Y., Yan, Z., Yuan, C., Liu, C. and Li, J. 2009. Early Paleozoic to Devonian multiple-accretionary model for the Qilian Shan, NW China. *Journal of Asian Earth Sciences*, **35**, 323–333, https://doi.org/10.1016/j.jseaes.2008.10.001

Xu, X., Wang, F. *et al.* 2005. Late Quaternary sinistral slip rate along the Altyn Tagh fault and its structural transformation model. *Science in China Series D: Earth Sciences*, **48**, 384–397, https://doi.org/10.1360/02yd0436

Xu, X., Zuza, A.V., Yin, A., Lin, X., Chen, H. and Yang, S. 2020. Permian plume-strengthened Tarim lithosphere controls the Cenozoic deformation pattern of the Himalayan–Tibetan orogen. *Geology*, **49**, 96–100, https://doi.org/10.1130/G47961.1

Yang, J., Xu, Z., Zhang, J., Chu, C.-Y., Zhang, R. and Liou, J.-G. 2001. Tectonic significance of early Paleozoic high-pressure rocks in Altun–Qaidam–Qilian Mountains, northwest China. *Geological Society of America, Memoirs*, **194**, 151–170, https://doi.org/10.1130/0-8137-1194-0.151

Yao, W., Liu-Zeng, J. *et al.* 2019. Reevaluation of the Late Pleistocene slip rate of the Haiyuan fault near Songshan, Gansu Province, China. *Journal of Geophysical Research: Solid Earth*, **124**, 5217–5240, https://doi.org/10.1029/2018JB016907

Yin, A. 2010. Cenozoic tectonic evolution of Asia: a preliminary synthesis. *Tectonophysics*, **488**, 293–325, https://doi.org/10.1016/j.tecto.2009.06.002

Yin, A. and Harrison, T.M. 2000. Geologic evolution of the Himalayan–Tibetan orogen. *Annual Review of Earth and Planetary Sciences*, **28**, 211–280, https://doi.org/10.1146/annurev.earth.28.1.211

Yin, A. and Taylor, M.H. 2011. Mechanics of V-shaped conjugate strike-slip faults and the corresponding continuum mode of continental deformation. *GSA Bulletin*, **123**, 1798–1821, https://doi.org/10.1130/B30159.1

Yin, A., Kapp, P.A. *et al.* 1999. Significant late Neogene east–west extension in northern Tibet. *Geology*, **27**, 787–790, https://doi.org/10.1130/0091-7613(1999)027<0787:SLNEWE>2.3.CO;2

Yin, A., Rumelhart, P. *et al.* 2002. Tectonic history of the Altyn Tagh fault system in northern Tibet inferred from Cenozoic sedimentation. *GSA Bulletin*, **114**, 1257–1295, https://doi.org/10.1130/0016-7606(2002)114<1257:THOTAT>2.0.CO;2

Yin, A., Manning, C.E., Lovera, O., Menold, C.A., Chen, X. and Gehrels, G.E. 2007. Early Paleozoic tectonic and thermomechanical evolution of ultrahigh-pressure (UHP) metamorphic rocks in the northern Tibetan Plateau, northwest China. *International Geology Review*, **49**, 681–716, https://doi.org/10.2747/0020-6814.49.8.681

Yin, A., Dang, Y.Q., Zhang, M., Chen, X.H. and McRivette, M.W. 2008*a*. Cenozoic tectonic evolution of the Qaidam basin and its surrounding

Downloaded from http://jgs.lyellcollection.org/ by GSL Maintenance User on July 7, 2021

regions (Part 3): structural geology, sedimentation, and regional tectonic reconstruction. *GSA Bulletin*, **120**, 847–876, https://doi.org/10.1130/B26232.1

Yin, A., Dang, Y.Q. *et al.* 2008*b*. Cenozoic tectonic evolution of Qaidam basin and its surrounding regions (Part 1): the southern Qilian Shan–Nan Shan thrust belt and northern Qaidam basin. *GSA Bulletin*, **120**, 813–846, https://doi.org/10.1130/B26180.1

Yu, J., Pang, J. *et al.* 2019. Mid-Miocene uplift of the northern Qilian Shan as a result of the northward growth of the northern Tibetan Plateau. *Geosphere*, **15**, 423–432, https://doi.org/10.1130/GES01520.1

Yu, J.-X., Zheng, W.-j. *et al.* 2017. Late Quaternary strike-slip along the Taohuala Shan-Ayouqi fault zone and its tectonic implications in the Hexi Corridor and the southern Gobi Alashan, China. *Tectonophysics*, **721**, 28–44, https://doi.org/10.1016/j.tecto.2017.09.014

Yu, L., Xiao, A., Wu, L., Tian, Y., Rittner, M., Lou, Q. and Pan, X. 2017. Provenance evolution of the Jurassic northern Qaidam Basin (West China) and its geological implications: evidence from detrital zircon geochronology. *International Journal of Earth Sciences*, **106**, 2713–2726, https://doi.org/10.1007/s00531-017-1455-z

Yu, X.J., Fu, S.T. *et al.* 2014. Paleomagnetism of Eocene and Miocene sediments from the Qaidam basin: implication for no integral rotation since the Eocene and a rigid Qaidam block. *Geochemistry, Geophysics, Geosystems*, **15**, 2109–2127, https://doi.org/10.1002/2014GC005230

Yuan, D.-Y., Champagnac, J.-D. *et al.* 2011. Late Quaternary right-lateral slip rates of faults adjacent to the lake Qinghai, northeastern margin of the Tibetan Plateau. *GSA Bulletin*, **123**, 2016–2030, https://doi.org/10.1130/B30315.1

Yuan, D.Y., Ge, W.P. *et al.* 2013. The growth of northeastern Tibet and its relevance to large-scale continental geodynamics: a review of recent studies. *Tectonics*, **32**, 1358–1370, https://doi.org/10.1002/tect.20081

Yuan, Z., Liu-Zeng, J. *et al.* 2018. A 6000-year-long paleoseismologic record of earthquakes along the Xorkoli section of the Altyn Tagh fault, China. *Earth and Planetary Science Letters*, **497**, 193–203, https://doi.org/10.1016/j.epsl.2018.06.008

Zhang, H.P., Craddock, W.H. *et al.* 2012. Magnetostratigraphy of the Neogene Chaka basin and its implications for mountain building processes in the north-eastern Tibetan Plateau. *Basin Research*, **24**, 31–50, https://doi.org/10.1111/j.1365-2117.2011.00512.x

Zhang, P.Z., Shen, Z. *et al.* 2004. Continuous deformation of the Tibetan Plateau from global positioning system data. *Geology*, **32**, 809–812, https://doi.org/10.1130/G20554.1

Zhang, P.Z., Molnar, P. and Xu, X.W. 2007. Late Quaternary and present-day rates of slip along the Altyn Tagh Fault, northern margin of the Tibetan Plateau. *Tectonics*, **26**, TC5010, https://doi.org/10.1029/2006TC002014

Zhang, Y.-P., Zheng, W.-J. *et al.* 2019. Late Pleistocene left-lateral slip rates of the Gulang Fault and its tectonic implications in eastern Qilian Shan (NE Tibetan Plateau), China. *Tectonophysics*, **756**, 97–111, https://doi.org/10.1016/j.tecto.2019.02.013

Zheng, D., Clark, M.K., Zhang, P., Zheng, W. and Farley, K.A. 2010. Erosion, fault initiation and topographic growth of the North Qilian Shan (northern Tibetan Plateau). *Geosphere*, **6**, 937–941, https://doi.org/10.1130/GES00523.1

Zheng, D., Wang, W. *et al.* 2017. Progressive northward growth of the northern Qilian Shan–Hexi Corridor (northeastern Tibet) during the Cenozoic. *Lithosphere*, **9**, 408–416, https://doi.org/10.1130/L587.1

Zheng, W., Zhang, H.P., Zhang, P.Z., Molnar, P., Liu, X.W. and Yuan, D.Y. 2013*a*. Late Quaternary slip rates of the thrust faults in western Hexi Corridor (Northern Qilian Shan, China) and their implications for northeastward growth of the Tibetan Plateau. *Geosphere*, **9**, 342–354, https://doi.org/10.1130/GES00775.1

Zheng, W., Zhang, P. *et al.* 2013*b*. Transformation of displacement between strike-slip and crustal shortening in the northern margin of the Tibetan Plateau: evidence from decadal GPS measurements and late Quaternary slip rates on faults. *Tectonophysics*, **584**, 267–280, https://doi.org/10.1016/j.tecto.2012.01.006

Zheng, W.J., Zhang, P.Z., Ge, W.P., Molnar, P., Zhang, H.P., Yuan, D.Y. and Liu, J.H. 2013*c*. Late Quaternary slip rate of the South Heli Shan Fault (northern Hexi Corridor, NW China) and its implications for northeastward growth of the Tibetan Plateau. *Tectonics*, **32**, 271–293, https://doi.org/10.1002/tect.20022

Zhuang, G., Hourigan, J.K., Ritts, B.D. and Kent-Corson, M.L. 2011. Cenozoic multiple-phase tectonic evolution of the northern Tibetan Plateau: constraints from sedimentary records from Qaidam basin, Hexi Corridor, and Subei basin, northwest China. *American Journal of Science*, **311**, 116–152, https://doi.org/10.2475/02.2011.02

Zuza, A. and Yin, A. 2016. Continental deformation accommodated by non-rigid passive bookshelf faulting: an example from the Cenozoic tectonic development of northern Tibet. *Tectonophysics*, **677**, 227–240, https://doi.org/10.1016/j.tecto.2016.04.007

Zuza, A., Cheng, X. and Yin, A. 2016. Testing models of Tibetan Plateau formation with Cenozoic shortening estimates across the Qilian Shan–Nan Shan thrust belt. *Geosphere*, **12**, 501–532, https://doi.org/10.1130/GES01254.1

Zuza, A., Levy, D., Wu, C., Li, B., Chen, X., Wang, Z. and Xiong, X. 2018*a*. Underthrusting and duplexing beneath the northern Tibetan Plateau and the evolution of the Himalayan–Tibetan orogen. *Lithosphere*, **11**, 209–231, https://doi.org/10.1130/L1042.1

Zuza, A., Wu, C. *et al.* 2018*b*. Tectonic evolution of the Qilian Shan: an early Paleozoic orogen reactivated in the Cenozoic. *GSA Bulletin*, **130**, 881–925, https://doi.org/10.1130/B31721.1